Huang *et al. Microstructures* 2024;4:2024027
DOI: 10.20517/microstructures.2023.102

Microstructures

Review

Open Access

Check for updates

Na-deficient P2-type layered oxide cathodes for practical sodium-ion batteries

Yu Huang[1], Weixiong Zeng[2], Kui Li[2], Xiaobo Zhu[1]

[1]College of Materials Science and Engineering, Changsha University of Science and Technology, Changsha 410114, Hunan, China.
[2]Tuo Feng New Energy Co., Ltd., Changsha 410323, Hunan, China.

Correspondence to: Prof. Xiaobo Zhu, College of Materials Science and Engineering, Changsha University of Science and Technology, 960, 2nd Section, Wanjiali RD (S), Changsha 410114, Hunan, China. E-mail: xbzhu@outlook.com

How to cite this article: Huang Y, Zeng W, Li K, Zhu X. Na-deficient P2-type layered oxide cathodes for practical sodium-ion batteries. *Microstructures* 2024;4:2024027. https://dx.doi.org/10.20517/microstructures.2023.102

Received: 29 Dec 2023 **First Decision:** 20 Feb 2024 **Revised:** 29 Feb 2024 **Accepted:** 19 Mar 2024 **Published:** 15 May 2024

Academic Editor: Shaobo Cheng **Copy Editor:** Yanbing Bai **Production Editor:** Yanbing Bai

Abstract

Sodium-ion batteries (SIBs) have attracted enormous attention as candidates in stationary energy storage systems, because of the decent electrochemical performance based on cheap and abundant Na-ion intercalation chemistry. Layered oxides, the workhorses of modern lithium-ion batteries, have regained interest for replicating their success in enabling SIBs. A unique feature of sodium layered oxides is their ability to crystallize into a thermodynamically stable P2-type layered structure with under-stoichiometric Na content. This structure provides highly open trigonal prismatic environments for Na ions, permitting high Na^+ mobility and excellent structural stability. This review delves into the intrinsic characteristics and key challenges faced by P2-type cathodes and then comprehensively summarizes the up-to-date advances in modification strategies from compositional design, elemental doping, phase mixing, morphological control, and surface modification to sodium compensation. The updated understanding presented in this review is anticipated to guide and expedite the development of P2-type layered oxide cathodes for practical SIB applications.

Keywords: Sodium-ion batteries, layered structure, Na deficiency, P2-type, modification strategies, sodium compensation

INTRODUCTION

Electrochemical energy storage is critical in mitigating climate change by accelerating the integration of

renewable energy sources and transportation electrification[1]. As a representative, the lithium-ion battery (LIB), first commercialized in 1991 by Sony, has dominated the market of portable electronics and electric vehicles ever since. LIBs are now extending to grid energy storage applications, maximizing their role in combating climate change. However, their large-scale applications raise concerns about the availability and affordability of LIB-related critical minerals, including Li, Co, and Ni[2]. Therefore, low-cost battery chemistries are in high demand.

Among the alternative battery technologies, sodium-ion batteries (SIBs) have attracted great interest because of their appreciable performance afforded by the similar "rock-chair" intercalation chemistry, as shown in Figure 1A, utilizing extremely abundant and low-cost Na^+ as the charge carrier. The charge carrier is in high concentrations in both electrolytes and cathodes. Moreover, unlike the reliance of costly Ni and Co in the state-of-the-art LIB cathodes, the types of active Na-containing cathode compounds are much more diverse in structures and compositions[3]. Transition metals (TMs), such as Ti, V, Cr, Mn, Fe, Co, Ni, and Cu, all can serve as the active redox media[4]. As presented in Figure 1B, according to the earth's abundances[5] and world reserves of these metals[6], the shift to SIBs can dramatically mitigate the concerns of resource shortage. Compared to LIBs, the SIB chemistry promises reduced cost for not only electrolytes and cathodes but also other battery components such as the anode current collector (expensive copper foil is replaced by aluminum, as Na does not alloy with aluminum) and even shipping/storing because of the overdischarge tolerance of SIBs[7]. Apart from the cost advantages, the weak solvation capability of Na^+ and higher thermal stability of the electrolyte salt afford additional all-climate potential for SIBs, which is highly demanded for large-scale energy storage applications[8]. However, due to the heavier weight (22.9 g mol^{-1} *vs.* 6.9 g mol^{-1} for Li^+) and higher reduction potential of Na^+ [-2.71 V *vs.* SHE (standard hydrogen electrode) compared to -3.01 V *vs.* SHE for Li^+/Li], SIBs commonly show lower specific energy. Also, from the perspective of intercalation reaction, the much larger size of Na^+ (1.02 Å *vs.* 0.76 Å for Li^+) tends to cause sluggish solid-state diffusion and larger dimensional changes of the host structures[9,10]. Therefore, the development of SIBs with high specific capacity, high operating voltage, high rate capability, and long lifespan remains challenging.

Akin to the situation in LIBs, the performance and cost of SIBs are also largely dependent on the cathode materials. Currently, the most common cathode materials for SIBs include layered oxides, polyanionic compounds, Prussian blue analogs, and organic compounds. Each type has its own unique set of advantages and disadvantages. For example, polyanionic compounds generally have open three-dimensional skeletons, affording excellent structural stability. The inductive effect of polyanions also contributes to high redox voltage. However, they also suffer from low capacity and complex synthesis. Structural stability poses a challenge for Prussian blue analogs, despite the high ion conductivity. Organic compounds promise high flexibility for molecular design and environmental friendliness. However, their electronic conductivity is normally poor, and there is also the problem of easy dissolution in organic electrolytes[11]. Due to the enlarged size mismatch between Na^+ and the first-row TM ions, almost all TMs can readily form sodium layered oxides with a general formula of Na_xTMO_2[12]. Compositional variety, easy synthesis, and other merits, such as high specific capacity and high volumetric density, make layered oxides very attractive for SIBs[13]. The corresponding redox potential ranges of Na_xTMO_2 based on these TMs are presented in Figure 1C[14]. Sodium layered oxides mainly involve two thermodynamic polymorphs, namely P2- and O3-type phases. Although P2-type cathodes are deficient in Na content (typically ranging from 0.6 to 0.7) that requires additional Na supplement to achieve full-cell application, the intrinsically lower Na^+ diffusion barrier and better moisture tolerance of P2-type cathodes still make them very competitive for enabling high-performance SIBs. The intensive research activities on SIBs and P2-type layered oxides are reflected by the fast-growing publications found on the Web of Science with the topics of "*sodium ion batteries*" and

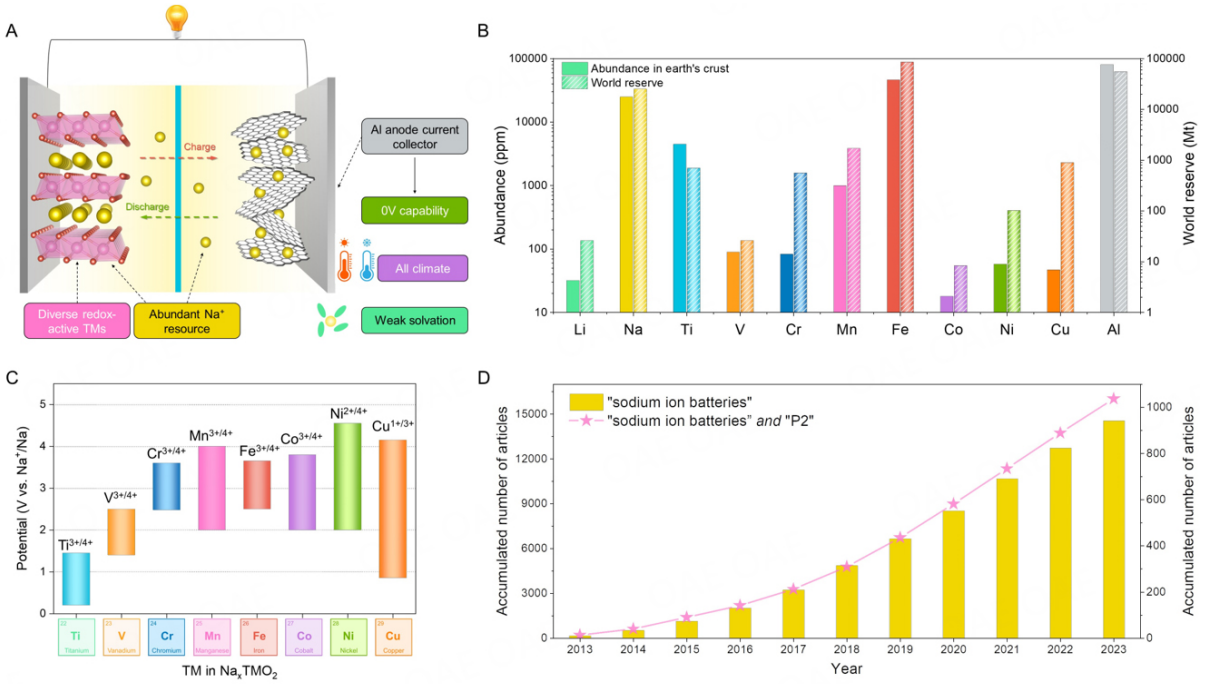

Figure 1. (A) Schematic illustration of a typical SIB using a layered oxide cathode and a hard carbon anode; (B) Abundances of the key metals involved in LIBs and/or SIBs in earth's crust and their world reserves as of 2023 (Mt = million metric tons). Data acquired from[5,6]; (C) The redox couples in Na_xTMO_2 compounds with their corresponding potential range. Data acquired from[14]; (D) Accumulated publications from the Web of Science with the topic of "sodium ion batteries" and "sodium ion batteries P2" in the year range of 2013 to 2023.

"*sodium ion batteries P2*", as shown in Figure 1D. Recently, Wang *et al.* demonstrated a 1.3 Ah pack cell using a P2-type cathode and a hard carbon anode[15]. The pouch cell showed a cell-level energy density of 165 Wh kg^{-1} with reasonable cycling stability (over 92% capacity retention after 100 cycles). This stimulates further interest in researching and developing P2 cathode materials towards commercialization. To chart a course for future development of P2-type cathode materials, here we start with an overview of P2-type materials in terms of their structural characteristics, then discuss the key challenges hindering their application and the up-to-date progress in combating these issues, and eventually offer perspectives and recommendations for future research.

STRUCTURAL FEATURES OF P2-TYPE OXIDES

The research on layered oxides can date back to 1958 when $LiCoO_2$ was first synthesized[16]. Its Li intercalation capability was initially investigated by Mizushima *et al.*[17] in 1980, leading to the remarkable success of LIBs. On the other hand, its sodium analog, Na_xCoO_2, was first reported by Fouassier *et al.*[18]. In 1981, Delmas *et al.*[19] studied the Na intercalation behavior of Na_xCoO_2, which was extended to other sodium layered oxides such as Na_xCrO_2[20], Na_xNiO_2[20], and Na_xTiO_2[21]. With a general formula of A_xTMO_2 (A = Li or Na), the term "layered structure" vividly describes their crystallography, in which alkali metals and TMs distribute orderly in the oxygen close packing lattices, forming TMO_2 slabs separated by Li^+/Na^+ layers. When the size difference between alkali metal ions and TM ions becomes significant, such ordered atomic arrangement is energetically favored as it reduces lattice constraints. Consequently, layered structures are more prevalent in the crystal chemistry of Na_xMO_2 due to the larger differences between Na^+ and trivalent TM ions. In fact, all sodium $NaTMO_2$ (TM = Ti, V, Cr, Mn, Fe, Co, and Ni) materials can crystallize into layer structures, while $LiTMO_2$ compounds, including $LiTiO_2$, $LiMnO_2$, and $LiFeO_2$, tend to

form metal-mixing rock-salt structures.

Different from the stoichiometric Li in $LiTMO_2$, the enhanced covalency of the TM-O bond attributed to the stronger ionic character of the Na-O stabilizes the tetravalent TM ions. Therefore, Na-deficient layered oxides can be thermodynamically stable. This leads to use of the more general formation of Na_xTMO_2 instead of $NaTMO_2$ and richer polymorphism along with the variation in Na content. Figure 2A compares the crystal structure of Na-deficient P2 structure (typically $0.6 \leq x \leq 0.7$) with another common polymorph of O3 phase that contains higher Na content (normally $0.8 \leq x \leq 1$). Such structural classification was introduced by Delmas *et al.* based on the Na coordination environment and oxygen stacking rules[22]. The letters "P" and "O" represent the trigonal prismatic coordination and octahedral coordination environments of Na ions, respectively. Furthermore, a prime symbol (′) can be added to indicate a monoclinic/orthorhombic distortion. Three possible dense stacking positions of O atoms in a MeO_2 layer are donated as A, B and C. The number "2" or "3" refers to the quantity of oxygen stacking layers in one unit cell. Specifically, P2 represents prismatic coordination of Na^+ between TMO_2 layers with an oxygen stacking sequence of "ABBA.....". In contrast, O3 structure accommodates Na^+ with octahedral sits and has an oxygen layer stacking in a manner of "ABCABC". The connection between the alkali content and the polymorph (oxygen stacking sequence) can be explained by the electrostatic interaction. Lower Na contents increase the electrostatic repulsion between oxygen layers, favoring the direct facing of oxygen layers (AA, BB) with larger interlayer distance in the case of P2 structure. Conversely, Na-rich layered oxides tend to crystallize into an O3 polymorph[23]. The Na^+ content is not the only parameter to determine the polymorphs. Zhao *et al.* proposed a "cationic potential" rule to rationalize the prediction of P2 and O3 structures [Figure 2B][24]. According to the theory, a larger cationic potential indicated stronger TM electron cloud extension and interlayer electrostatic repulsion resulting in the P2-type structure, with more covalent TM-O bonds and an increased $d_{(O\text{-}Na\text{-}O)}$ distance. Alternatively, a larger mean Na ionic potential, achieved by increasing Na content, increased the shielding of the electrostatic repulsion between the TMO_2 slabs, promoting the O3-type structure.

Compared to O3 structure, P2 is privileged for fast and reversible Na^+ (de)intercalation. This is not only related to the expanded interlayer accommodating Na^+ but, more importantly, the direct Na^+ migration pathway in P2 structure. Na^+ migrates from prismatic to neighboring sites through open square bottlenecks surrounded by four oxygen ions, which are much less repulsive than the interstitial tetrahedral sites in the O3 structure. Katcho *et al.* experimentally and theoretically compared the Na^+ mobility in P2 and O3 structures with an identical composition of $Na_{2/3}Fe_{2/3}Mn_{1/3}O_2$[23]. The computed activation energies (*E*a) are 127 and 201 meV for P2 and O3 phases, respectively [Figure 2C]. Correspondingly, the diffusion coefficients are 1.28×10^{-12} and 6.43×10^{-14} $cm^2\ s^{-1}$. The more open framework of P2 phase not only enables a lower diffusion barrier but is also more easily preserved after sodium extraction[25], although a partial P2-O2/OP4 phase transition was reported[4,26-28]. Whereas the O3 phase always transforms to the P3 phase via gliding of the MeO_2 slabs that results from the presence of intermediate tetrahedral sites between two octahedral sites [Figure 2D][29,30]. As a result, P2-type layered oxides generally show better rate performance and cyclic stability[31,32].

In addition, the higher Na content in O3 structures corresponds to stronger basicity, leading to much more severe hygroscopicity than not only P2 counterparts but even the well-known air-sensitive Ni-rich LIB cathodes[33,34]. For example, more carbonates were formed on a typical O3 cathode of $NaNi_{1/3}Fe_{1/3}Mn_{1/3}O_2$ in a much shorter time (4.64 wt.% after 1,000 h) compared with Li-NMC811 (0.39 wt.% after one year) [Figure 2E][35,36]. The consequences of generating sodium residues on the cathode are detrimental in many aspects. First, the spontaneous desodiation from the layered structure leads directly to the loss of active Na

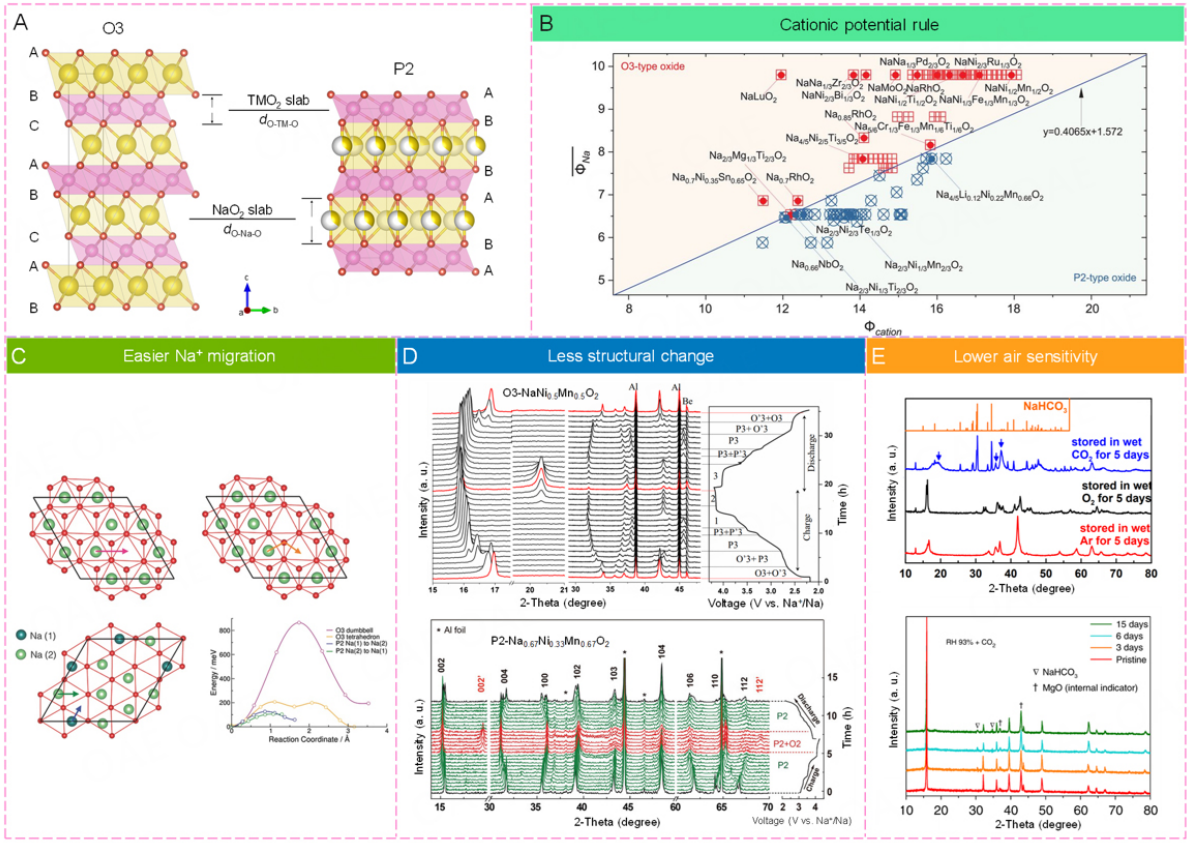

Figure 2. Comparisons of O3 and P2 cathode materials from different aspects. (A) Crystal structure of P2 and O3 layered oxides; (B) Cationic potential rule to determine the formation of P2 and O3 structures. Reproduced with permission, Copyright 2020[24], American Association for the Advancement of Science; (C) Na diffusion pathways and barriers in P2 and O3 cathodes. Reproduced with permission, Copyright 2017[23], Wiley-VCH; (D) Structural evolutions of P2 and O3 cathodes under electrochemical Na extraction/insertion. Reproduced with permission, Copyright 2022[26], Wiley-VCH. Reproduced with permission, Copyright 2018[29], Wiley-VCH; (E) Air storage properties of typical P2 and O3 cathode materials. Reproduced with permission, Copyright 2018[35], American Chemical Society. Reproduced under terms of the CC-BY license, Copyright 2020[37], The Authors, Nature Publishing Group.

inventory. Second, the insulating sodium compounds on the surface block the sodium diffusion and electron pathway. Additionally, the basic sodium residues defluorinate polyvinylidene difluoride (PVDF) binders, damaging the electrode-coating process. Therefore, the high air-sensibility of O3 cathodes is one of the biggest challenges hindering their practical applications, which will dramatically increase the difficulty and cost in production, handling, transportation, storage, *etc*. Although the concern of air instability still exists in P2 cathodes, the problem is much less significant [Figure 2E] and P2 cathodes can be water-processable with the design of proper TM components[37-39].

CHALLENGES OF P2-TYPE OXIDES

Despite the instinct advantages of P2-type cathodes over O3 counterparts in terms of smaller Na^+ diffusion barrier, better structural reversibility, and higher water stability, P2-type layered oxides still face some critical challenges that need to be solved prior to their practical application:

(1) Structural deformation. Although the more open crystal framework offers P2-type cathodes better structural stability, the nature of the layered structure still poses a risk of irreversible structural transformations due to slab gliding and lattice distortion upon the removal/insertion of Na^+[40,41]. The

structural stability of the P2 host relies significantly on the content of Na^+, which plays a crucial role in mitigating electrostatic repulsions between the TMO_2 slabs. Along with the desodiation in the charging process, the reduced shielding effect of Na^+ triggers the slab gliding. This phenomenon leads to a structural transition from P-type to O-type stackings[42]. It was found that at deep desodiation ($x \approx 0.25$), the cathode undergoes a P2-O2 and/or P2-OP4 phase transition with various Na^+/vacancy ordering structures[43-45]. In the case of deep discharge to 1.5 V, an orthogonal phase was found to be produced and co-existed with P2 phase[46]. The repeated phase transition and separation processes can break down electrode particles by inducing numerous intragranular cracks due to the massive strain at phase boundaries[47-49], plaguing the electrochemical performance.

(2) Interfacial instability. An unstable electrode/electrolyte interface often interplays with the structural degradation, causing rapid electrochemical deterioration. First, the structural deformation is generally more severe at the surface of a cathode due to the higher state of charge and direct contact with the electrolyte. As a result, severe atomic rearrangement drives irreversible phase reconstruction, forming ion-blocking rock-salt/spinel phases. Furthermore, the chemical/electrochemical oxidation of the electrolyte produces acidic species, which attack the metal oxide cathode, causing TM dissolution and O loss. TM dissolution is a well-known aging mechanism in LIBs[50,51], which is serious for cathodes containing Jahn-Teller active TM ions, such as Mn^{3+}, Ni^{3+}, and Fe^{4+}. At the same time, these ions are extensively involved in sodium layered oxides, including P2 ones.

(3) Insufficient ambient stability. P2 cathodes are less hygroscopic than O3 materials because of their lower basicity. This allows better ambient stability, especially in humid conditions. However, these cathodes still suffer undesirable side reactions upon prolonged ambient exposure. Apart from Na^+/H^+ exchange process being less severe than that of O3 materials, a prevailing explanation to the air instability of P2 cathodes is the large interlayers that allow the insertion of foreign species such as water[52] and carbonate groups[53]. Recently, Zuo *et al.* elaborated on the structural/chemical transformations of P2 cathodes in moist air[37]. They confirmed that Na^+/H^+ exchange dominated the compensation of Na^+ extraction and hydration. At the same time, CO_2 was found to increase the acidity at the particle surface and accelerate the Na^+ loss rather than being inserted into the P2 structure. The authors further offered an empirical rule for estimating the air stability of P2 oxides, where the involvement of higher electrochemical-potential TM ions makes Na^+ extraction difficult, leading to better air stability.

(4) Na deficiency. The Na deficiency in P2 oxides contributes to the open crystal framework and low hygroscopicity, but it also poses a challenge for their practical application. As the common anode materials (e.g., hard carbon) are Na-free, the insufficient Na inventory greatly limits the capacity and energy density of P2 cathode-based full batteries. This is further aggravated due to the consumption of active Na in forming passivating solid electrolyte interphase (SEI) layers on the anode. As a result, P2 cathodes rely on sodium compensation in assembling practical full cells, which can be realized through anode pre-sodiation[54,55], cathode oversodiation[56,57], introduction of self-sacrificial sodiation reagents[58-63], *etc.* Cost, safety, and effectiveness are important from the perspective of industrialization.

ADVANCES IN MODIFICATION STRATEGIES

P2-type layered oxides exhibit compelling advantages but encounter persistent constraints, as discussed above. To propel the advancement beyond current bottlenecks, researchers have proposed various modification strategies focusing on compositional design, elemental doping, phase mixing, morphological control, surface modification, and sodium compensation [Figure 3]. These efforts have yielded promising results with the potential to unlock the full potential of P2-type materials for high-performance SIBs.

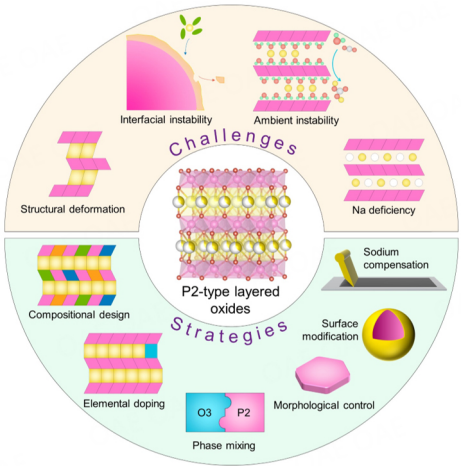

Figure 3. Key challenges and improvement strategies of P2-type layered cathode materials for SIBs.

Compositional design

Although Na^+ can easily form layered structure with all the first-row TMs due to the significant size difference between Na^+ and TM ions, only a few elements such as Co[64], Mn[65], and V[66] were demonstrated to be synthesized into P2 structure via solid-state reactions. This could be explained by the instability of their tetravalent states. Single TM P2-type oxides typically show low capacities and multiple plateaus due to complex Na^+/vacancy ordering. For example, an *in situ* X-ray diffraction (XRD) experiment conducted by Berthelot *et al.* revealed nine potential drops separated by either potential plateaus or sloping curves in the Na content range of $0.45 \leq x \leq 0.90$ for P2-Na_xCoO_2, corresponding to nine ordered phases[67]. P2-Na_xMnO_2 was reported to have a high specific capacity (*ca.* 140 mAh g^{-1})[68]. However, strains and distortions caused by Jahn-Teller active Mn^{3+} rapidly destroyed the crystal framework, leading to severe capacity drop.

In the effort to remove multiple plateaus and improve the average voltage and capacity, P2-type layered oxides have evolved to binary and multiple TM systems[69]. For example, Voronina *et al.* synthesized $Na_{0.6}Co_{0.78}Ru_{0.22}O_2$ using a combustion method [Figure 4A], and the specific capacity of the first discharge reached 163 mAh g^{-1} [Figure 4B] with no Na^+/vacancy ordering superstructures detected within the P2 phase, followed by a P2-OP4 phase transition under deep desodiation[70]. The increased capacity was attributed to additional Ru^{4+}/Ru^{5+} and $O^{2-}/(O_2^{n-})$ redox reactions. However, Co and Ru are both costly and scarce, undermining the sustainability benefits of SIBs. In this regard, Co-free or low-Co formulas have gained much interest[71], leading to a range of representative binary/ternary P2-phase compositions such as $Na_{2/3}Ni_{1/3}Mn_{2/3}O_2$[72-74], $Na_{2/3}Fe_{1/2}Mn_{1/2}O_2$[4], $Na_{2/3}Mn_{1/2}Fe_{1/4}Co_{1/4}O_2$[75], and $Na_{2/3}Mn_xNi_{x-1/3}Co_{4/3-2x}O_2$[76]. Lee *et al.* found that P2 phase can stably exist with the sodium content range of from 1/3 to 2/3 for P2-phase $Na_xNi_{1/3}Mn_{2/3}O_2$, which transferred to a more stable O2 phase when x approaches 0[27]. However, the cut-off voltage had to be set at 4.1 V (*vs.* Na^+/Na) to ensure stable cycling, delivering a reversible capacity below 90 mAh g^{-1}. Lu *et al.* detailed the structural evolution of P2-$Na_{2/3}Ni_{1/3}Mn_{2/3}O_2$ using in situ XRD[43]. It was found that P2-O2 phase transition occurred at a Na content of less than 1/3 (at a voltage of about 4.1 V), which was accompanied by a large volume change (about 23%). This answered the rapid capacity decay. The high-voltage operation of P2-$Na_xNi_{1/3}Mn_{2/3}O_2$ can be stabilized by metal substitutions. Liu *et al.* suggested that phase transition was controlled by the amount and distribution of Na ions retained in the lattice[77]. As shown in Figure 4C, a P2-$Na_{2/3}Mn_{1/2}Ni_{1/6}Co_{1/3}O_2$ was synthesized from $Na_{2/3}Mn_{2/3}Ni_{1/3}O_2$ and $Na_{2/3}Mn_{1/3}Co_{2/3}O_2$. The ternary P2 structure was found to remain stable with 0.17 Na ions, resulting in an ultra-low strain of 1.9% in volume, guaranteeing excellent cyclability [Figure 4D]. Moreover, the authors demonstrated the universality of this strategy, where P2-$Na_{2/3}Mn_{1/2}Ni_{1/6}Fe_{1/3}O_2$ and P2-$Na_{2/3}Mn_{7/12}Ni_{1/4}Fe_{1/6}O_2$

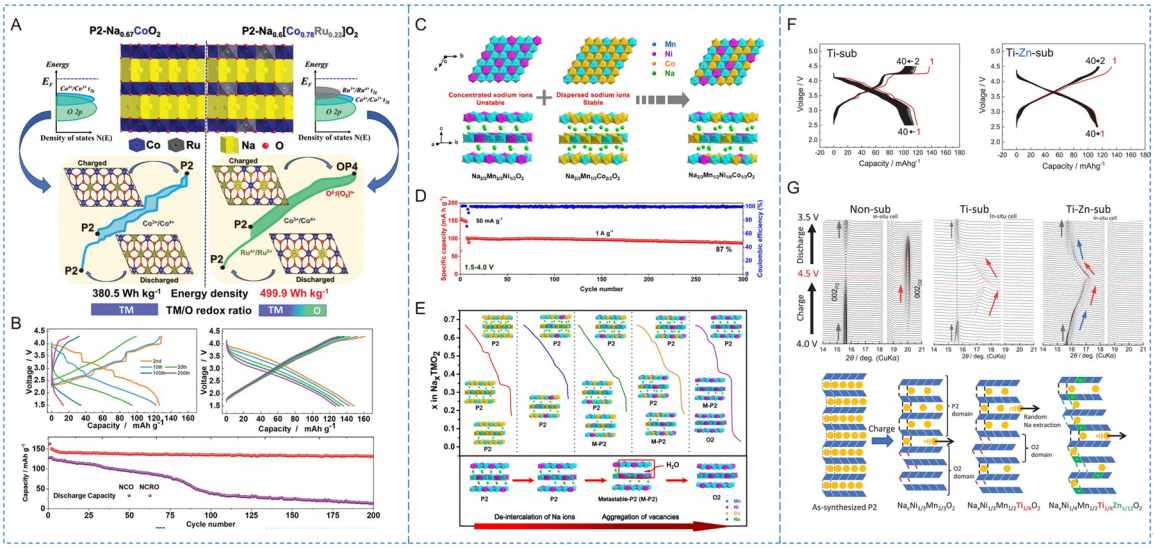

Figure 4. (A) Schematic illustration of structure, phase transitions, and corresponding reaction mechanisms for P2-$Na_{0.67}CoO_2$ and P2-$Na_{0.6}Co_{0.78}Ru_{0.22}O_2$; (B) Electrochemical performance of P2-$Na_{0.67}CoO_2$ and P2-$Na_{0.6}Co_{0.78}Ru_{0.22}O_2$. Reproduced with permission, Copyright 2023[70], Wiley-VCH; (C) Schematic illustration of the synthesis of P2-$Na_{2/3}Mn_{1/2}Ni_{1/6}Co_{1/3}O_2$; (D) Cycling stability of P2-$Na_{2/3}Mn_{1/2}Ni_{1/6}Co_{1/3}O_2$; (E) Schematic illustration of the phase transitions for P2-$Na_{2/3}Mn_xNi_{x-1/3}Co_{4/3-2x}O_2$ ($1/3 \leq x \leq 2/3$). Reproduced with permission, Copyright 2021[77], Wiley-VCH; (F) Voltage profiles and electrochemical performance of Ti-substituted and Ti-Zn-substituted P2 cathodes; (G) Selected operando XRD patterns and schematic illustrations of structural change mechanisms for these cathodes. Reproduced with permission, Copyright 2023[86], Wiley-VCH.

were also synthesized and did not transfer to O2 or OP4 phase when charging to 4.4 V [Figure 4E]. The involvement of non-active metals such as Ti, Mg, Zn, Al, and Li was also proven to alleviate structural evolutions[78-81]. For example, $Na_{2/3}Ni_{1/3}Mn_{1/2}Ti_{1/6}O_2$ permitted a much higher reversible capacity of 127 mA h g^{-1} within the voltage range of 4.5-2.5 V at a current density of 12.1 mA g^{-1}[81]. Recently, Zou *et al.* reported a zero-strain (0.53% volume change) P2-$Na_{2/3}Li_{1/6}Co_{1/6}Mn_{2/3}O_2$ cathode, which showed an excellent capacity retention of 95.8% after 250 cycles at 1 C[82]. The inactive monovalent Li^+ and active trivalent Co^{3+} were suggested to help stabilize the Mn-O bond by reducing Mn^{3+}/Mn^{4+} redox. Liu *et al.* proposed the co-substitution of inactive Mg and Ti elements to activate anionic redox reaction while maintaining excellent structural stability with a minor volume change of only 0.3%[83].

Further multi-elementalization leads to the creation of high-entropy (HE) layered oxides, which have attracted increasing attention in recent studies[84]. The entropy effect that promotes the metal disordering in the TM slabs greatly alleviates the phase segregation, permitting sloping voltage curves and excellent electrochemical properties. Wang *et al.* revealed the entropy effect on the electrochemical stability by comparing three different P2 cathodes: $Na_{0.67}Mn_{0.55}Ni_{0.21}Co_{0.24}O_2$, $Na_{0.67}Mn_{0.45}Ni_{0.18}Co_{0.24}Ti_{0.1}Mg_{0.03}O_2$, and $Na_{0.67}Mn_{0.45}Ni_{0.18}Co_{0.18}Ti_{0.1}Mg_{0.03}Al_{0.04}Fe_{0.02}O_2$ with low, medium, and high configurational entropy, respectively[85]. The HE one showed less structural transformation and Mn dissolution upon cycling in an expanded voltage range (1.5-4.6 V). Similarly, Cheng *et al.* reported a multiple metal-substituted P2-$Na_{0.7}Li_{0.03}Mg_{0.03}Ni_{0.27}Mn_{0.6}Ti_{0.07}O_2$, which delivered a reversible capacity (134 mAh g^{-1}), a high working voltage (3.57 V), and excellent cycling and rate performance[26]. However, without a precise understanding of the atomic arrangements and functionalities, the involvement of multiple elements could increase the unpredictability of the electrode materials. Kubota *et al.* challenged the necessity of HE by proposing a selective dual-substitution of Ti^{4+} for Mn^{4+} and Zn^{2+} (Mg^{2+}, Cu^{2+}) for Ni^{2+} in P2-$Na_{2/3}Ni_{1/3}Mn_{2/3}O_2$[86]. As presented in Figure 4F, the Ti-sub cathode still exhibited stepped voltage curves, whereas the further dual-substitution with divalent metals effectively smoothed the voltage curves. Correspondingly, *in situ* XRD

analysis [Figure 4G] revealed suppressed phase separation from pristine P2 cathode to Ti-substituted cathode and almost monotonous solid solution for dual-substituted $Na_{2/3}Ni_{1/4}Mn_{1/2}Ti_{1/6}Zn_{1/12}O_2$. It should be noted that the high-proportional metal substitution also reduces the specific capacities of P2 cathodes. In short, compositional design normally involves various elements that have rather high concentrations, which not only greatly affect both the crystal/electronic structure of the material and, hence, the reaction mechanism, but the selection of the elementals also needs to consider the cost efficiency and sustainability, since the high usage of costly elementals such as Co and Ru will sacrifice the key advantage of SIBs.

Elemental doping

The substitution of high-content active or inactive elementals in the compositional design can effectively reduce Na^+ vacancy ordering arrangement, contributing to the improved electrochemical performance. However, heavy metal substitution also renders considerable capacity and/or voltage sacrifice. Also, the involvement of high-content cations such as Co^{3+}, Fe^{3+}, and Ti^{4+} is believed to undermine the moisture stability of P2 oxides[37]. Therefore, it is compelling to lower the concentration of substitutive ions. Generally, the introduction of elementals with less than approximately 5 at.% can be deemed elemental doping[87].

Cation dopants can substitute both Na and TM ions, playing different roles during charge and discharge. For example, Zhang *et al.*[88] doped P2-$Na_{0.67}MnO_2$ with Mo-doped to avoid the phase transition and Jahn-Teller effect of Mn^{3+}. The resultant P2-$Na_{0.67}Mn_{0.97}Mo_{0.03}O_2$ exhibited a high specific capacity of 169.7 mAh g^{-1} and improved cycling stability with 84% capacity retention after 100 cycles at 50 mA g^{-1}. Wang *et al.* investigated the effect of K^+ doping in P2-$Na_{0.612}K_{0.056}MnO_2$[89]. The large-sized K^+ ions were preferably placed in the prismatic Na^+ sites sharing edges with MnO_6 octahedra, enlarging the Na-O-Na interlayer space while reducing the distances of adjacent MnO_2 slabs [Figure 5A]. P2-$Na_{0.612}K_{0.056}MnO_2$ exhibited a capacity of 240.5 mAh g^{-1} based on the high utilization of Mn^{3+}/Mn^{4+} redox, retaining 98.2% capacity after 100 cycles [Figure 5B]. Detailed structural analyses revealed that the reinforced interaction in the MnO_2 layers restricted the slab gliding, suppressing the OP4 phase generation even at high desodiated state [Figure 5C].

Elemental doping is also an important strategy to unlock the anionic redox. The extra capacity enabled by anionic redox reaction also remakes an opportunity for SIBs to compete with LIBs in terms of energy density. Ma *et al.* first identified the oxygen activity of P2-Type $Na_{0.78}Ni_{0.23}Mn_{0.69}O_2$[90]. Unlike the Li-rich cathode materials known for anionic redox reaction, the introduction of extra sodium in TM layers is not feasible due to the mismatch. Shen *et al.* synthesized a P2-$Na_{0.76}Ca_{0.05}[Ni_{0.23}\square_{0.08}Mn_{0.69}]O_2$ cathode material [Figure 5D][91]. The pillar effect of Ca^{2+} ions in Na layers enhanced anionic redox reversibility upon charge/discharge [Figure 5E]. Correspondingly, P2-O2 phase transition was much suppressed [Figure 5F]. Fu *et al.* proposed a dual-site doping of P2-type $Na_{0.67}Ni_{0.33}Mn_{0.67}O_2$, where Mg^{2+} replaced Ni^{2+} in the TM layers and Ca^{2+} tended to pillar the Na layers[92]. A synergetic effect was discovered in co-doped P2-$Na_{0.62}Ca_{0.025}Ni_{0.28}Mg_{0.05}Mn_{0.67}O_2$, which showed suppressed oxygen redox and Ni^{4+}/Ni^{3+} redox reactions at the high-voltage region, permitting enhanced structural stability. Despite the surge in research on anionic redox, formidable challenges such as rapid material degradation, voltage fade, and oxygen release pose significant barriers to practical implementation of anionic redox materials[93,94]. New mechanistic understandings and novel strategies progress rapidly in this area. For example, regulating anionic redox through the combination of metal ligands in layered sulfides[95], stabilizing lattice oxygen redox through spin singlet state[96], and inhibiting excess lattice oxygen oxidation through the comprehensive strengthening of the TM-O bond by the introduction of Al^{3+}[97] have effectively improved the rechargeability of the anionic redox.

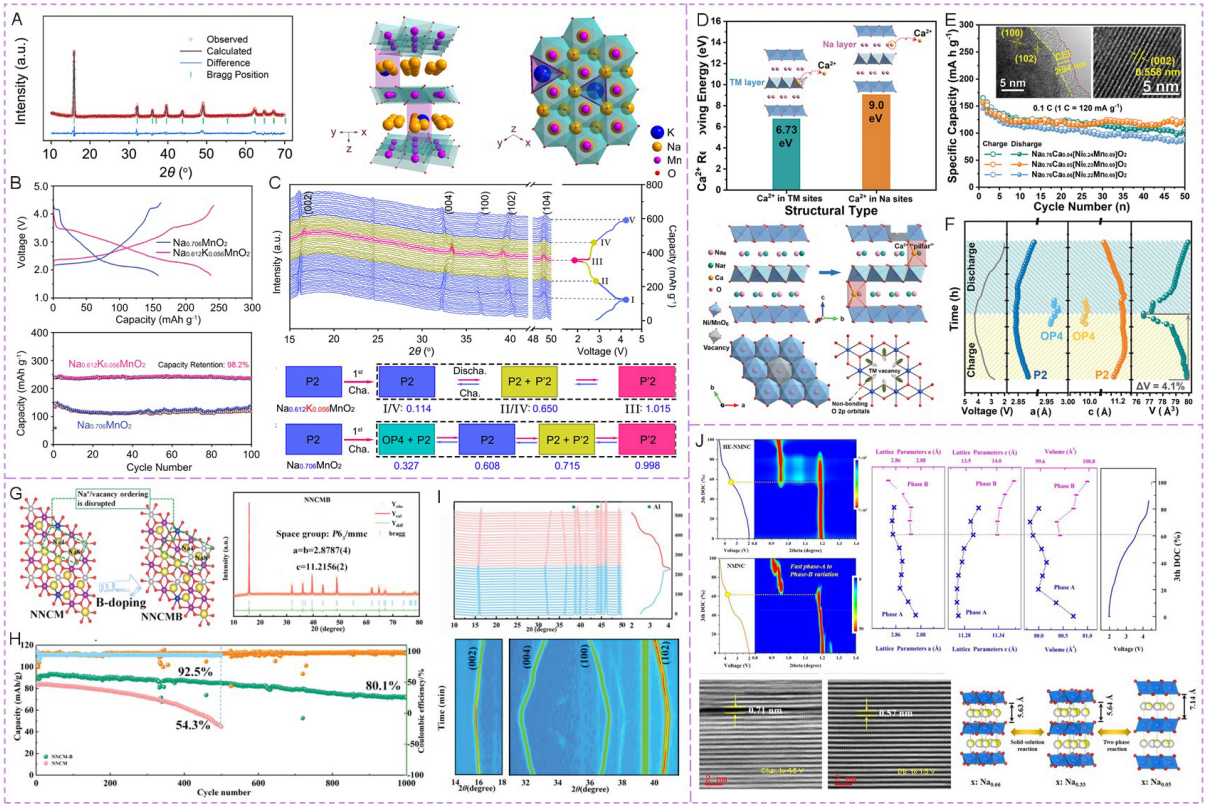

Figure 5. (A) XRD pattern of $Na_{0.612}K_{0.056}MnO_2$ with Rietveld refinement and the corresponding structural model; (B) Typical charge/discharge curves of $Na_{0.612}K_{0.056}MnO_2$ and $Na_{0.706}MnO_2$ at 20 mA g^{-1} in the third cycle and their cycling performance at 50 mA g^{-1}; (C) *In situ* XRD patterns of $Na_{0.612}K_{0.056}MnO_2$ and schematic diagram of the phase transitions. Reproduced under terms of the CC-BY license, Copyright 2021[89], The Authors, Nature Publishing Group; (D) Computational and experiential investigations of $Na_{0.76}Ca_{0.05}[Ni_{0.23}\square_{0.08}Mn_{0.69}]O_2$; (E) Electrochemical properties of P2 cathodes doped with different Ca^{2+} concentrations; (F) Structural evolution of P2-$Na_{0.76}Ca_{0.05}[Ni_{0.23}\square_{0.08}Mn_{0.69}]O_2$ during charge and discharge. Reproduced with permission, Copyright 2021[91], Wiley-VCH; (G) Structural model and XRD pattern of P2-$Na_{0.67}Ni_{0.3}Co_{0.1}Mn_{0.6}O_{1.94}(BO_3)_{0.02}$; (H) Cycling performance of pristine and BO_3^{3-}-modified P2 cathodes; (I) Structural evolution of BO_3^{3-}-modified P2 cathode. Reproduced with permission, Copyright 2022[99], Wiley-VCH; (J) A comparison of the structural evolution between undoped and HE-doped P2 cathodes, Copyright 2023[103], Elsevier B.V.

Doping species are not limited to cations; anion dopants such as F^- and BO_3^{3-} have also been used to overcome the drawbacks of P2 cathodes. Liu *et al.* investigated a charge compensation mechanism of F^- doping in P2-$Na_{2/3}Ni_{1/3}Mn_{2/3}O_2$[98]. F-substitution triggered partial reduction of Mn from Mn^{4+} to Mn^{3+}, which perturbed the Ni^{2+}/Mn^{4+} cation ordering and activated the Mn^{3+}/Mn^{4+} redox for additional capacities. Wang *et al.* incorporated triangular BO_3^{3-} into the P2 structure to form $Na_{0.67}Ni_{0.3}Co_{0.1}Mn_{0.6}O_{1.94}(BO_3)_{0.02}$ [Figure 5G], which enabled a capacity retention of 80.1% after 1,000 cycles at 2 C [Figure 5H][99]. Structural characterizations confirmed that configuration acted as a strong pillar to address the TM layer sliding and H_2O insertion issues, guaranteeing reduced volume change (1.8%) and facilitating Na^+ transportation [Figure 5I]. Anion dopants are often introduced together with cation dopants, such as Al^{3+}/F^-[100], Ca^{2+}/F^-[101], and Mg^{2+}/F^-[102]. For instance, Cui *et al.* reported *ex-situ* F and *in-situ* Mg dual doping method to obtain P2-$Na_{0.524}Mg_{0.146}Ni_{0.15}Fe_{0.20}Mn_{0.65}F_{0.05}O_{1.95}$[102]. F doping modified the bond energy of O-O and TM-O, allowing the reduction of interatomic distance of TM and the expansion of the interlayer spacing. As a result, capacity fading caused by structural deformation and Jahn-Teller effect was mitigated. Meanwhile, electrochemically introduced Mg-Mg dimers could act as pillars to widen the interlayer gaps and enhance the mechanical strength, further inhibiting phase transition and layer sliding.

Co-doping of multiple ions also gained research interest due to the potential of the synergistic effect of multi-elements. Ma *et al.* proposed HE doping strategy with five equal contents (1 at.%) of cations to achieve a novel $Na_{0.667}Mn_{0.667}Ni_{0.167}Co_{0.117}Ti_{0.01}Mg_{0.01}Cu_{0.01}Mo_{0.01}Nb_{0.01}O_2$ (HE-NMNC)[103]. Instead of a sudden P2-O2 transition, the HE-NMNC showed a gentle and reversible phase variation in a wider voltage region [Figure 5J], delivering a capacity of 111 mAh g^{-1} at 5 C and retaining around 130 mAh g^{-1} after 100 cycles at 1 C.

Employing minor components to fundamentally modify the electrochemical properties of P2 oxides presents a very attractive and feasible strategy for commercialization, which is also widely used for the LIB industry. However, it is crucial to acknowledge that elemental doping can have both positive and negative effects. While it may enhance cycling stability, it might also compromise capacity. Therefore, a comprehensive evaluation and mechanistic understanding of both advantages and limitations is essential to identify the optimal doping strategy.

Phase mixing

Designing mixing-phase cathode materials is a promising approach to addressing some of the limitations of single-phase materials and achieving enhanced performance. The intergrowth of thermodynamically stable P2 and O3 phases is the most investigated mixing phase system. As discussed above, O3 phase has higher Na content and high specific capacity, which can be introduced to advance P2 for better performance and practicality.

Lee *et al.* first reported the layered O3/P2 intergrowth cathode in Li-substituted $Na_{1-x}Li_xNi_{0.5}Mn_{0.5}O_2$, where x is the Li content[104]. As Li content rose from 0 to 0.5, the P2 phase fraction increased, while the O3 phase fraction decreased. This resulted in a significant improvement in both capacity and rate capability. However, the O3-P3 phase transition could not be completely avoided due to a large amount of the O3 phase. This resulted in a significant capacity loss within 20 cycles. In contrast, Guo *et al.* introduced minor O3 phases into the P2 host material[105]. The P2-majority $Na_{0.66}Li_{0.18}Mn_{0.71}Ni_{0.21}Co_{0.08}O_2$ exhibited a remarkable increase in capacity (200 compared to 125 mAh g^{-1} for the single P2 phase). Additionally, the composite demonstrated superior rate capability and impressive cycling stability across a wide voltage range of 1.5-4.5 V (75% capacity retention after 150 cycles). Recently, Huang *et al.* demonstrated the construction of Li-enriched O3 nanodomains in the P2 phase matrix (P2/Li-O3, Figure 6A), which was designed to overcome the interlayer gliding and to suppress the multiple-phase transitions in P2-$Na_{0.67}Mn_{0.67}Ni_{0.33}O_2$ [Figure 6B][106]. As can be seen, Li substitution is responsible for generating biphasic materials, where Li mainly substitutes the TM ions, maintaining the P2 structure, while some Li ions occupy Na sites to tune the Na/TM ratio, generating O3 phase[107].

Beside Li substitution, the introduction of Mg^{2+}[108], Ti^{4+}[109], or multiple ions[110-115] was also demonstrated to enable P2/O3 intergrowth. For example, Liang *et al.* reported a Fe-Mg-Li co-substitution to prepare P2/O3 $Na_{7/9}Ni_{2/9}Mn_{4/9}Fe_{1/9}Mg_{1/9}Li_{1/9}O_2$[111]. Compared to pure P2 phase, the heterostructure showed suppressed P2-O2 phase evolution at high potential and much less microcrack generation over cycling. Gao *et al.* investigated the formation mechanisms of biphasic layered oxides from the perspective of cationic potential theory, where the existence of P2/O3 biphasic structure was experimentally and theoretically non-uniform element distribution within a micrometer scale [Figure 6C and Figure 6D][114]. With a reversible P2-Z/O3-P3-O3′ phase transition [Figure 6E], the biphasic $Na_{0.7}Ni_{0.2}Cu_{0.1}Fe_{0.2}Mn_{0.5}O_{2-\delta}$ overperformed P2 and O3-type analogs in terms of rate capability and cycling stability [Figure 6F].

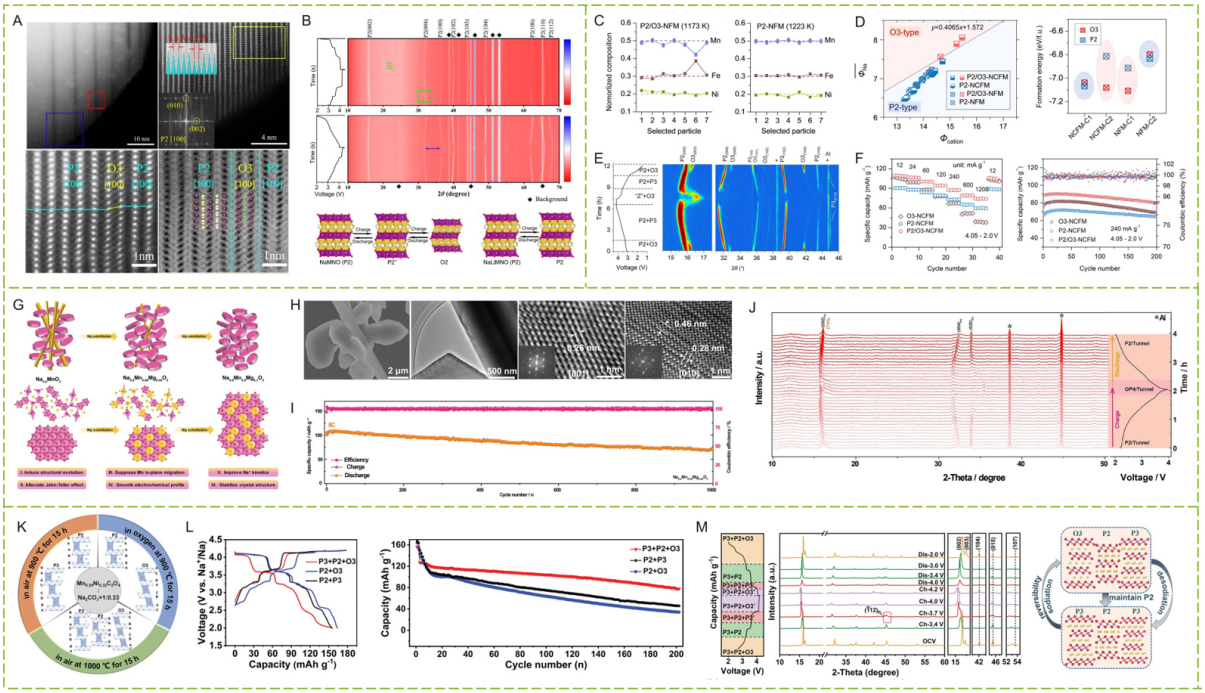

Figure 6. (A) High angle annular dark field scanning transmission electron microscope (HAADF-STEM) images of P2/Li-O3 sample; (B) Structural evolution of P2/Li-O3 during the first charge/discharge process in comparison with pure P2 cathode. Reproduced with permission, Copyright 2022[106], Elsevier B.V.; (C) Normalized composition of Ni, Fe, and Mn in selected particles of P2/O3 and P2 materials; (D) Calculated cationic potentials and formation energies rationalizing the structure-composition relationship; (E) *In situ* XRD revealing the structural evolution of P2/O3 cathode; (F) Electrochemical performance of O3, P2, and P2/O3 cathodes. Reproduced with permission, Copyright 2022[114], Elsevier B.V.; (G) Schematic illustration of structural evolution driven by Mg substitution contents in $Na_{0.6}Mn_{1-x}Mg_xO_2$ (x = 0.05, 0.1); (H) Scanning electron microscopy (SEM), transmission electron microscopy (TEM), and high-resolution (HR-TEM) images with corresponding fast Fourier transform (FFT) electron diffraction (ED) patterns of P2/tunnel $Na_{0.6}Mn_{0.95}Mg_{0.05}O_2$; (I) Long-cycling stability of the P2/tunnel cathode; (J) Structural evolution of the P2/tunnel cathode revealed *in situ* XRD patterns. Reproduced with permission, Copyright 2023[120], Wiley-VCH; (K) Schematic diagram of the formation conditions of mixed-phase materials; (L) Electrochemical performance of the P3/P2/O3 tri-phase cathode compared to biphasic P3/P2 and P2/O3 materials. Reproduced with permission, Copyright 2022[124], Wiley-VCH.

Apart from P2/O3 heterostructure, recent research progress has witnessed the creation of other mixed-phase systems, such as layered P2/P3/spinel[116], P2/tunnel[117-120], P2/O'3[9], P2/T[121], P2/O2[122], P2/spinel[123], and P3/P2/O3[124]. By adjusting magnesium content in $Na_{0.6}Mn_{1-x}Mg_xO_2$, Xiao *et al.* realized the control of phase structure from P2/tunnel structure to P2 structure [Figure 6G][120]. $Na_{0.6}Mn_{0.95}Mg_{0.05}O_2$, with a reasonable structure component ratio (92.6% P2 and 7.4% tunnel, Figure 6H), displayed an excellent capacity retention of 71.3% after 1,000 cycles at 5 C [Figure 6I]. A gentle structural evolution was identified [Figure 6J]. Li *et al.* introduced an undoped method to prepare P3/P2/O3-$Na_{0.674}Ni_{0.319}Mn_{0.590}O_2$ by varying the calcination temperature and gas atmosphere [Figure 6K][124]. The tri-phase material showed improved electrochemical performance compared to biphasic P2/O3 and P2/P3 cathodes [Figure 6L]. The enhanced structural stability was explained by a structural constraint effect, where the grain boundaries suppressed the continuous slip of the TMO_2 layer [Figure 6M].

The design of multiple-phase systems creates more opportunities for developing high-performance P2-related cathode materials by combining the attractive features of other phases and even achieving unexpected synergistic effects of mixed-phase structures. However, there are also associated challenges of mixing phases, such as phase segregation, possible antagonistic effects, and increased complexity, which need to be carefully explored.

Morphological control

A central challenge in current LIBs lies in the massive, often several percent, expansive strain induced by Li intercalation within the crystal structure. Materials prone to abrupt phase transitions further concentrate this strain, amplifying the lattice mismatch at the sharp interface between lithiated and delithiated phases. The interface can not only impede ion transfer but also serve as nucleation points of microcracks, given the inherent hardness and brittleness of most metal oxide battery materials[48,49,51,125]. In view of the much larger ionic size of Na^+, the kinetic and stability issues become much more serious. Morphology optimization, such as the designs of nanostructures[126-128], hierarchical structures[129-133], core-shell/concentration-gradient configurations[134-138], single crystals[139], and selective faceting[140,141], has been proved to be effective in combating these problems.

Shen *et al.* synthesized a P2-$Na_{0.76}Cu_{0.22}Fe_{0.30}Mn_{0.48}O_2$ cathode with a pearl necklace-like hierarchical nanostructure through electrospinning[127]. As suggested by the authors, the nano-necklace architecture involving very small secondary nanograins (50-150 nm) could expose rich active sites to electrolyte, thus shortening the ionic diffusion distance and alleviating the aggregation of nanoparticles upon repeated (de)sodiation [Figure 7A-C]. The importance of this nanostructure was demonstrated by the sensitivity of electrochemical performance toward the synthesis temperature [Figure 7D]. Peng *et al.* reported a hierarchical one-dimensional rod-like P2-$Na_{0.67}Ni_{0.23}Mg_{0.1}Mn_{0.67}O_2$ composed of nanoplate subunits [Figure 7E-G][130]. Such morphology was found to be preserved after cycling, while many cracks were presented in the common monodisperse particle [Figure 7H].

The design and application of nanostructures can both reduce the size of the electrode material, increase the electrode/electrolyte contact, and provide shorter transfer paths for off/electrons. However, nanostructured electrode materials encounter significant difficulties in practical applications. First, nanomaterials in their as-synthesized form are considerably low in the mass densities, translating into unsatisfactory volumetric energy densities. Second, the high surface area and porosity of nanostructured materials tend to stimulate the parasitic reactions with electrolytes, spoiling battery lifetime[142]. Therefore, research efforts have been devoted to the design and engineering of micron-sized single-crystal cathodes. Zuo *et al.*[143] developed a water-mediated method to convert bulk P2-$Na_{0.67}MnO_2$ into shale-like Na_xMnO_2 (S-NMO) with enlarged interlayer spacing [Figure 7I]. S-NMO exhibited only 1.96% volume change during charge/discharge, resulting in much improved electrochemical performance [Figure 7J]. Moreover, S-NMO showed excellent humidity tolerance, and the feasibility of the water-mediated strategy was further demonstrated by extending to other sodium layered oxides. Zhang *et al.* synthesized hexagonal-prism-like single-crystal P2-$Na_{0.66}Ni_{0.26}Zn_{0.07}Mn_{0.67}O_2$ featuring a high proportion of {001} facets [Figure 7K-Q] using a molten-salt-based method[140]. Such single-crystal morphology was suggested to reduce the gliding of TMO_2 slabs [Figure 7R]. This helped suppress the microcracks and associated electrolyte decomposition, guaranteeing much better electrochemical stability. Facet engineering can be coupled with other strategies. For example, Fu *et al.* combined crystal-facet modulation with an HE design[141]. The optimized P2 cathode exhibited outstanding cycling performance (87% capacity retention after 500 cycles at 120 mA g^{-1} and 75% after 2,000 cycles at 1.2 Ag^{-1}).

Surface modification

High interfacial stability of the electrode surface is a prerequisite for realizing long-lasting secondary batteries[144]. Due to the direct electrode-electrolyte contract and normally high states of charge at the cathode surface, P2 layered cathodes undergo significant surface reactivity and a sequential transformation of the surface structure during charging and discharging especially under high-voltage operation, leading to severe surface degradation[145]. As an effective strategy, surface modification can effectively shield the direct contact between P2 cathode materials and the electrolyte, thus reducing the side reactions between the

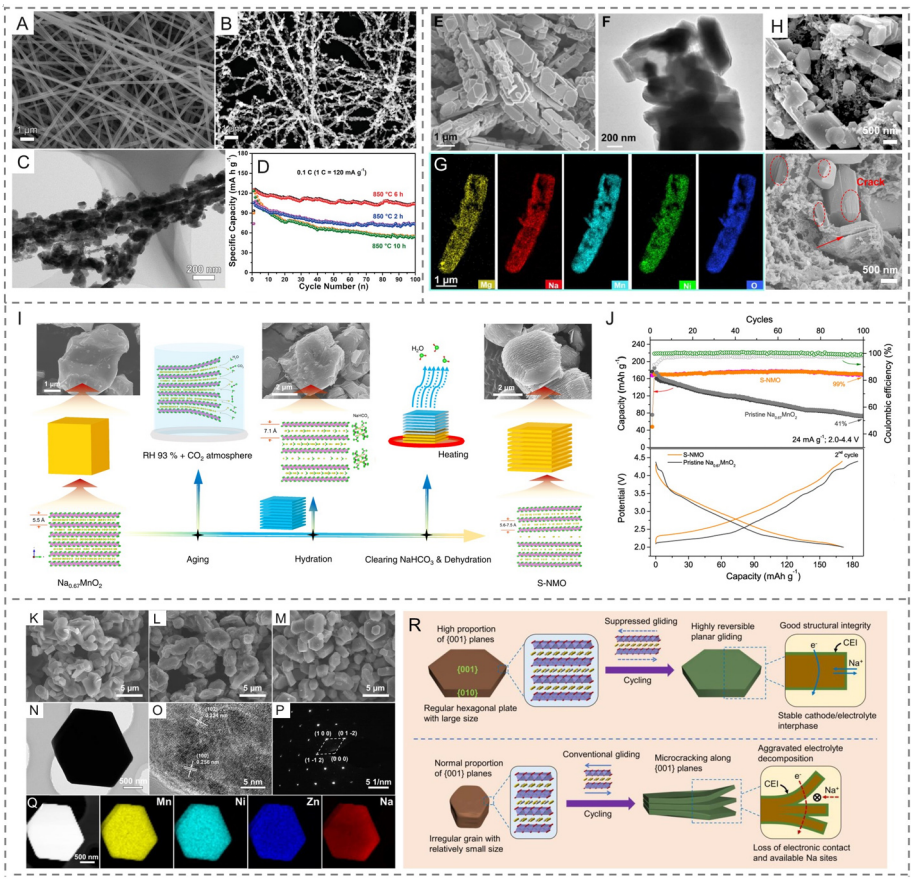

Figure 7. (A) SEM images of electrospun nanofibers; (B and C) SEM and TEM images of resultant $Na_{0.76}Cu_{0.22}Fe_{0.30}Mn_{0.48}O_2$ nano-necklaces; (D) Electrochemical performance of $Na_{0.76}Cu_{0.22}Fe_{0.30}Mn_{0.48}O_2$ calcinated at different conditions. Reproduced under terms of the CC-BY license, Copyright 2020[127], The Authors, Wiley-VCH; (E-G) SEM, TEM, and elemental mappings of hierarchical P2-$Na_{0.67}Ni_{0.23}Mg_{0.1}Mn_{0.67}O_2$; (H) SEM images of cycled P2 cathodes with hierarchical and bulk morphologies. Reproduced with permission, Copyright 2021[130], Elsevier B.V.; (I) Schematic illustration of the water-mediated strategy to prepare S-NMO; (J) Electrochemical properties of S-NMO and bulk P2-$Na_{0.67}MnO_2$. Reproduced under terms of the CC-BY license, Copyright 2021[143], The Authors, Nature Publishing Group. (K-M) SEM images of P2-$Na_{0.66}Ni_{0.26}Zn_{0.07}Mn_{0.67}O_2$ materials prepared by solid-state, coprecipitation, and combined coprecipitation and molten-salt methods; (N-Q) TEM, HR-TEM, ED pattern, and elemental mappings of the hexagonal single crystal; (R) Schematic illustration comparing the structural stability of primary particles with different proportions of {001} planes. Reproduced with permission, Copyright 2023[140], Elsevier B.V.

electrode material and the electrolyte and inhibiting the TM dissolution[41,146]. In addition, it can protect the P2 cathode from contacting carbon dioxide and water from the air to realize easier materials storage and processing[41].

With the chemical affinity, metal oxides are the most investigated coating species for sodium layered oxides including P2 ones[147,148]. For instance, Ren *et al.* coated P2-$Na_{2/3}Ni_{1/3}Mn_{2/3}O_2$ with ZrO_2, where Zr^{4+} partially doped into the layered (P2-NaNM@Zr) [Figure 8A and B][149]. The ZrO_2 coating layer was proven to prevent cathode-electrolyte interfacial reactions, suppressing electrolyte decomposition and the accumulation of associated byproducts. Meanwhile, Zr^{4+} modification was suggested to add "impurity-vibrational entropy" to host structure, which reduced P2-O2 phase transition and endorsed a zero-strain (1.18%) feature even when charged to 4.5 V. As a result, P2-NaNM@Zr cathode retained 77% of its capacity after 200 cycles at the rate of 5 C within the voltage range of 2.0-4.5 V [Figure 8C]. Similarly, Wan *et al.* modified Mg^{2+}-doped P2-$Na_{0.67}Ni_{0.33}Mn_{0.67}O_2$ with a ZrO_2 surface layer[150]. ZrO_2 coating was evidenced to inhibit the side reactions

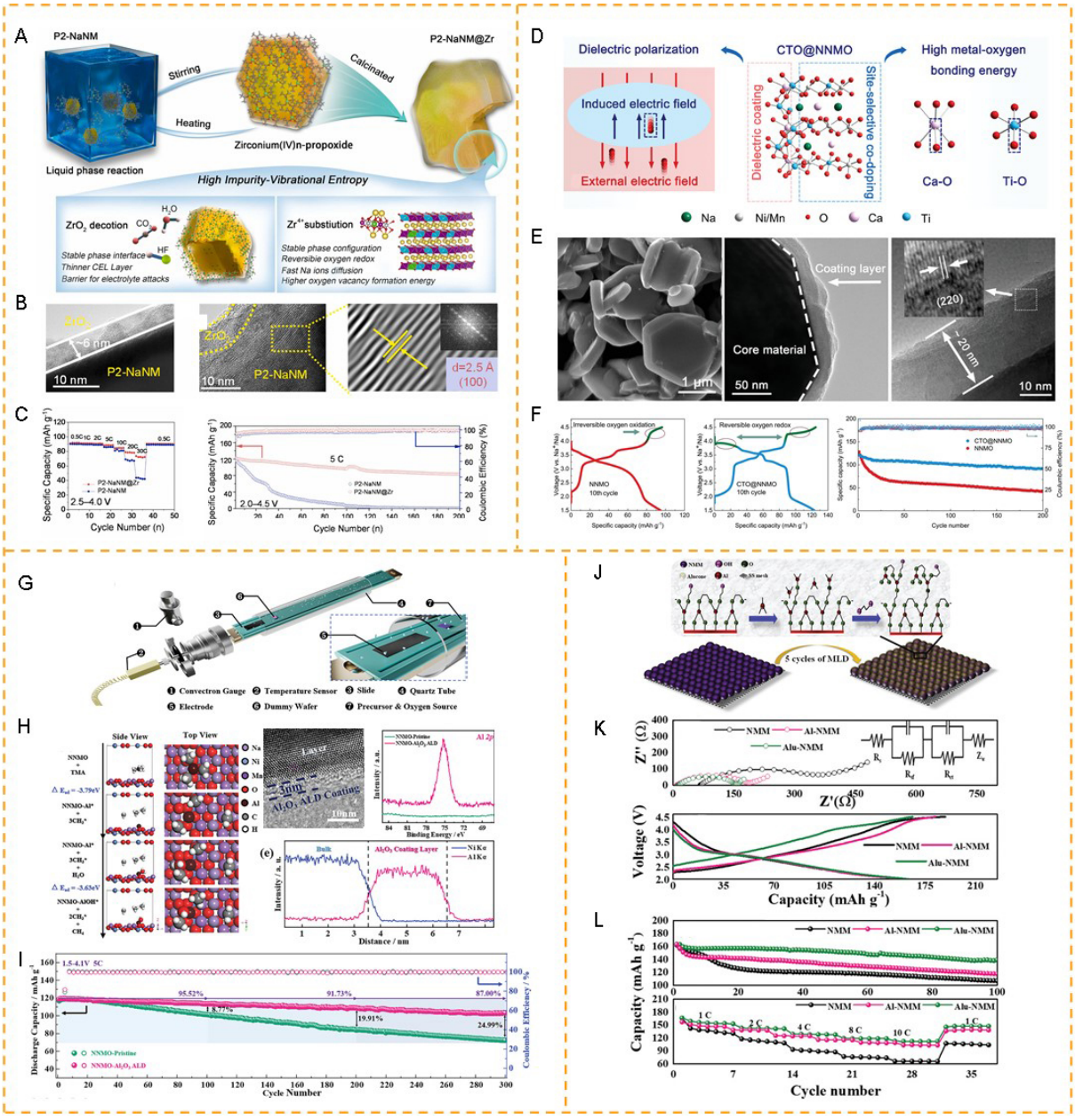

Figure 8. (A) Schematic illustration of the Zr modification process and effects on a P2 cathode; (B) TEM characterizations of the Zr-modified P2 cathode; (C) Rate and cycling performance of P2-NaNM@Zr in comparison with the bare P2-$Na_{2/3}Ni_{1/3}Mn_{2/3}O_2$. Reproduced with permission, Copyright 2022[149], Elsevier B.V.; (D) Schematic diagram of the oxygen loss suppressed by simultaneous dielectric surface coating and site-selective co-doping; (E) SEM and TEM characterizations of $CaTiO_3$-modified P2-$Na_{2/3}Ni_{1/3}Mn_{2/3}O_2$; (F) Voltage profiles and cycling performance of bare and $CaTiO_3$-modified P2-$Na_{2/3}Ni_{1/3}Mn_{2/3}O_2$. Reproduced with permission, Copyright 2023[151], Wiley-VCH; (G) Schematic illustration of the lab ALD facility; (H) Simulated diagram and characterizations of the ALD coating of Al_2O_3 on the surface of $Na_{2/3}Ni_{1/3}Mn_{2/3}O_2$; (I) cycling performance of unmodified and Al_2O_3-coated $Na_{2/3}Ni_{1/3}Mn_{2/3}O_2$ cathodes. Reproduced with permission, Copyright 2022[156], Wiley-VCH; (J) Schematic illustration of alucone coating introduced by MLD process on the surface of P2 oxides; (K) Nyquist spectra and charge-discharge curves of uncoated, Al_2O_3-coated, and alucone-coated P2-$Na_{0.66}Mn_{0.9}Mg_{0.1}O_2$; (L) Cycling and rate performance of these P2 cathodes. Reproduced with permission, Copyright 2020[158], Wiley-VCH.

at high voltages, contributing to better electrochemical stability. Besides, Xia *et al.* proposed a dielectric $CaTiO_3$ coating on P2-$Na_{2/3}Ni_{1/3}Mn_{2/3}O_2$ that also featured site-selective Ca/Ti co-doping, leading to a

synergy in suppressing dynamic oxygen evolution [Figure 8D and E][151]. It was confirmed that the coating layer inhibited not only the surface oxygen release but also the migration of bulk oxygen due to the reverse electric field created by the dielectric polarization. Correspondingly, the reversibility of anion redox reaction was largely improved as evidenced by voltage profiles and cycling stability [Figure 8F].

In general, the thickness, type, and uniformity of the coating layers are crucial in affecting the performance of the electrode materials. If the coating layer is too thick and/or unevenly/loosely wrapped, it can be detrimental to the ionic and electronic conductivity and/or insufficient in offering protection[152]. In response, atomic layer deposition (ALD) with Å-level control has attracted much attention for the deposition of uniform and conformal metal-oxide coatings on electrode surfaces[153-155]. Ji *et al.* found that the failure at the cathode-electrolyte interface was the dominant cause of capacity attenuation for P3/P2 biphasic $Na_{2/3}Ni_{1/3}Mn_{2/3}O_2$ [156]. To solve this problem, they explored ALD coating with four different metal oxides, including Al_2O_3, TiO_2, SnO_2, and WO_3. Figure 8G shows the schematic illustration of the ALD facility. The deposition process and outcome of Al_2O_3 on the surface of the $Na_{2/3}Ni_{1/3}Mn_{2/3}O_2$ was theoretically and experimentally investigated [Figure 8H]. The Al_2O_3 protection dramatically improved the cycle life of the cathode, permitting a capacity retention of 87.00% after 300 cycles at 5 C within a 1.5-4.1 V charge-discharge window [Figure 8I]. Zuo *et al.* reported a Al_2O_3@$Na_{0.67}Zn_{0.1}Mn_{0.9}O_2$ electrode by taking the advantages of both structural stabilization and surface passivation via Zn^{2+} substitution and Al_2O_3 ALD coating[157]. The ALD coating layer effectively alleviated the electrolyte decomposition and significantly improved the cycling performance of the P2 cathode. Similar to ALD, molecular layer deposition (MLD) can also deposit ultra-thin polymer or organometallic coatings while maintaining precise control over coating thickness and consistency[158]. Kaliyappan *et al.* first demonstrated alucone coating of P2-$Na_{0.66}Mn_{0.9}Mg_{0.1}O_2$ by the MLD method [Figure 8J][158]. The alucone-coated P2 cathode showed smaller charge transfer resistance and lower polarization than both uncoated and Al_2O_3-coated P2 counterparts [Figure 8K], corresponding to higher rate performance and longer cycling stability [Figure 8L].

Apart from the metal oxide coatings, other species such as carbon[159], metal fluorides[160], polyanionic compounds[161-165], and conductive polymers[166,167] have been extensively investigated to improve the surface/interface stability of P2 layered oxides. Surface/interface stability plays a pivotal role in determining the performance and stability of SIBs. At its core, surface modification aims to minimize harmful side reactions between the cathode and electrolyte, thereby boosting interface stability. Moreover, depending on the chosen coating species and surface treatment methods, surface modification can facilitate Na^+ diffusion, suppress detrimental phase transitions, and ultimately enhance the overall electrochemical performance. Despite its vast potential, surface modification faces challenges. For example, *ex situ* synthesis methods often struggle to achieve uniform coatings, compromising the effectiveness of the coating layer. Additionally, precise control of the coating thickness is crucial. While thicker oxide coatings provide enhanced stability, their inherently low electron conductivity can rapidly hinder performance if excessive. Striking this balance remains a bottleneck for large-scale implementation of this promising technology.

Sodium compensation

Most P2-type materials have low Na stoichiometry, which contributes to electrochemical and ambient stability but poses a problem to significantly reduce the accessible capacity in practical cells without additional active Na^+ sources. When tested in half cell, Na-deficient cathodes present abnormal initial coulombic efficiencies (ICEs) of higher than 100% due to the discharge back of more Na ions offered by the Na metal anode. However, there is generally no Na inventory from the practical anode. This issue was deteriorated by the further trapping and/or consumption of the limited Na^+ inventory in forming electrolyte-electrode interfaces, restricting the capacities and cyclability of the resultant cells[168-170]. The development of Na-rich P2-type oxides can partially relieve this problem[171-175], but critical limitations of Na

content in P2 oxides persist, and it could sacrifice the air stability of P2 compounds. Therefore, it is compelling to develop feasible sodium compensation strategies useful for not only P2 oxides but also many other Na-stoichiometric materials[63,176,177].

Various methods such as electrochemical pre-sodiation[178], direct sodium foil contact[179], anode pre-sodiation[55,180], cathode oversodiation[56,57], self-sacrificial sodiation additives[58-63] have been explored to solve the Na^+ inventory problem for different types of SIB cathode chemistries. Among them, the easy introduction of sacrificial reagents has gained enormous attention from the perspective of industrialization. Ideally, suitable sodium replenishers should feature high sodiation capacity, non-toxicity, moderate decomposition potential, and easy handling and synthesis. In 2013, Singh *et al.* proposed using NaN_3 as a sodium replenishing agent, which decomposed into compensating Na source and gaseous N_2 during initial charge[60]. This was also explored by Martinez De Ilarduya *et al.*[62]. The addition of 10 wt.% NaN_3 to P2-$Na_{0.67}Fe_{0.5}Mn_{0.5}O_2$ allowed a 60% increase in reversible capacity. However, the following studies found that NaN_3 decomposition caused porosity on the electrode surface. Moreover, in the selection of additives, not only the efficiency but also the sustainability must be considered. NaN_3 is highly toxic and explosive, hindering its practical application. Niu *et al.*[63] then proposed an efficient cathodic sodium supplement agent, $Na_2C_2O_4$ [Figure 9A], which had a high theoretical capacity of 400 mAh g^{-1} and could achieve a high capacity utilization of 99% [Figure 9B], which outperformed Na_2CO_3[181], Na_2NiO_2[57], and $Na_2C_4O_4$[182] with ratios of 20%, 22%, and 70%, respectively. Furthermore, the oxidation overpotential (2.44 V) of NaC_2O_4 could be reduced using a conductive additive with a high specific surface area. The sodiation additive boosted the capacity retention of hard carbon||P2-$Na_{2/3}Ni_{1/3}Mn_{1/3}Ti_{1/3}O_2$ full cell from 63% to 85% (200 cycles) and the energy density from 129.2 to 172.6 Wh kg^{-1}. In addition, other sodium replenishing agents have been investigated, such as $NaCrO_2$[61], $Na_4C_6O_6$[183], $Na_2C_6O_6$[184], $Na_2C_6H_2O_6$[176], EDTA-4Na[185] and DTPA-5Na[186], *etc.*, although not all of them were applied to P2 materials.

Guo *et al.* proposed spraying Na_2O_2 slurry on the surface of P2-$Na_{2/3}Ni_{1/3}Mn_{1/3}Ti_{1/3}O_2$ electrode as a sodium supplementary method [Figure 9C][187]. Na_2O_2 showed good chemical and storage stability under a dry atmosphere and had no negative effect on the electrochemical performance of the cathode. Compared to common blending process, this spraying method was suggested to avoid the incomplete decomposition of additives and the generation of porous electrodes due to gas release. As a result, the capacity, rate capability, and cycling stability of the hard carbon||P2-$Na_{2/3}Ni_{1/3}Mn_{1/3}Ti_{1/3}O_2$ full cell were considerably improved [Figure 9D]. While all the above-mentioned approaches require external Na sources, Zhang *et al.* reported the utilization of the residual alkali compounds of P2-$Na_{0.85}Li_{0.12}Ni_{0.22}Mn_{0.66}O_2$ by an acetic-acid treatment, which neutralized the surface alkali substance into sodium acetate (AC-Na) [Figure 9E][188]. This strategy transformed the detrimental substances into active Na reservoirs. The energy density of the cell optimized in this way was increased from 112 to 130 Wh kg^{-1}, and the soft-pack battery was also able to achieve capacity retention of 95.1% over 120 cycles.

Note that many additives release gases upon the supplement of active Na^+. This easily causes increase in the internal pressure and problematic inner contact. The development of gas-free cathode additives with high sodium availability is attractive for practical application. Liao *et al.* introduced Na_3PS_3O in a P2-$Na_{0.66}Ni_{0.26}Zn_{0.07}Mn_{0.67}O_2$ electrode using the solution casting method [Figure 9F][189]. Na_3PS_3O offered a sodiation capacity of over 300 mAh g^{-1} (60% capacity delivered below 4.0 V). More importantly, the decomposition products did not involve gaseous species, and the solid products were even found to be beneficial in suppressing electrolyte decomposition and oxygen release from the P2 cathode. The addition of Na_3PS_3O improved the energy density of the hard carbon||P2-$Na_{0.66}Ni_{0.26}Zn_{0.07}Mn_{0.67}O_2$ cell by 29.7% [Figure 9G]. The metrics (theoretical capacity, practical capacity, and decomposition potentials) of these

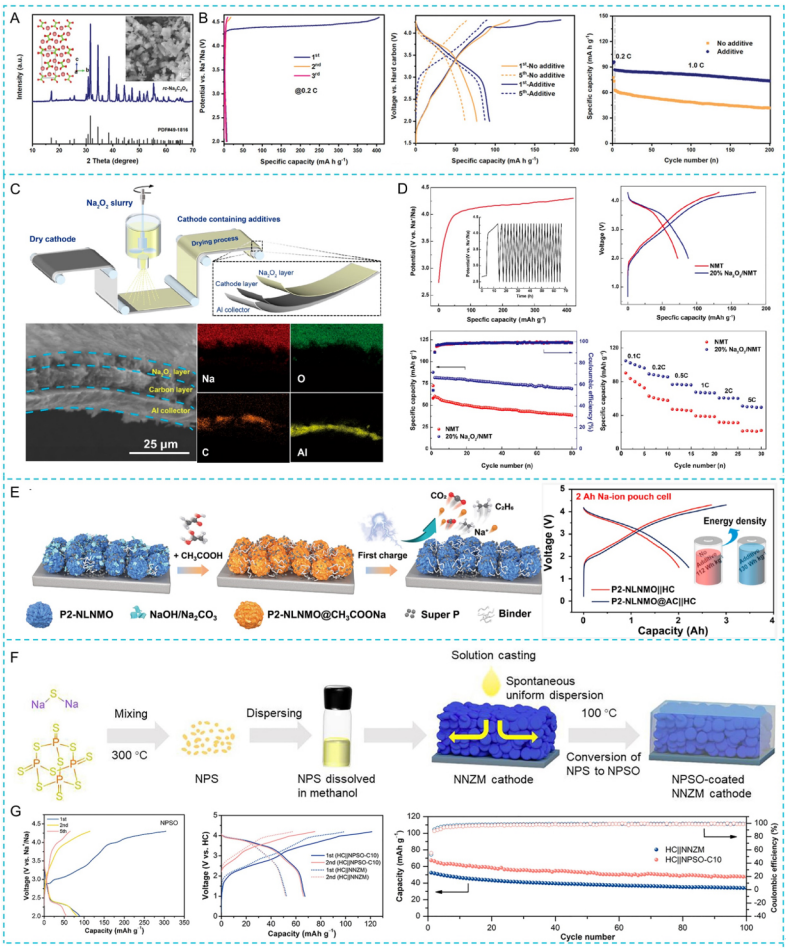

Figure 9. (A) Structural characteristics of $Na_2C_2O_4$; (B) Electrochemical properties of $Na_2C_2O_4$ and its application as a cathode sodium compensator. Reproduced with permission, Copyright 2020[63], Wiley-VCH; (C) Schematic illustration of the slurry spraying method to deposit Na_2O_2 sacrificial layer on the P2 electrode film and corresponding characterization of the resultant composite electrode; (D) Electrochemical properties of Na_2O_2 and its use as a cathode sodium compensator. Reproduced with permission, Copyright 2021[187], American Chemical Society; (E) Schematic illustration of the treatment of P2-$Na_{0.85}Li_{0.12}Ni_{0.22}Mn_{0.66}O_2$ with acetic acid and the role of the as-formed AC-Na as sodium reservoir. Reproduced with permission, Copyright 2021[188], American Chemical Society; (F) Schematic illustration of the preparation of Na_3PS_3O and Na_3PS_3O-cast P2-$Na_{0.66}Ni_{0.26}Zn_{0.07}Mn_{0.67}O_2$ electrode; (G) Electrochemical properties of Na_3PS_3O and its application as a sodium sacrificing additive. Reproduced with permission, Copyright 2022[189], Elsevier B.V.

typical pre-sodiation additives are summarized in Table 1.

SUMMARY AND OUTLOOK

SIBs are considered to be the most promising alternative or complementing energy storage technology to current LIBs due to the extremely abundant Na resource and a range of attractive characteristics such as the allowance of using aluminum foil as the anode current collector, easy desolvation of Na^+, 0 V capability, *etc.* These features make SIBs highly competitive especially in the scenario of large-scale stationary energy storage. P2-type layered cathodes could be a key enabler for the success of SIBs owing to their advantages of high structural reversibility, low Na^+ diffusion energy barrier, compositional diversity, acceptable humid stability, high volumetric density, easy synthesis, *etc.* However, many issues still hinder the practical application of P2 cathodes, which have been summarized into four aspects: structural deformation, interfacial instability, insufficient ambient stability, and Na deficiency. The progress in solving these problems has also been comprehensively reviewed from six categories, i.e., compositional design, elemental

Table 1. A comparison of typical cathode pre-sodiation additives

Additives	Theoretical capacity [mAh g^{-1}]	Practical capacity [mAh g^{-1}]	Decomposition potential [V *vs.* Na^+/Na]	Ref.
NaN_3	412	300	3.55	[60]
Na_3P	802	600	4.30	[56]
$Na_2C_2O_4$	400	394.6	4.41	[63]
Na_2CO_3	505	92	4.00	[181]
Na_2NiO_2	392.2	88.7	2.10	[57]
$Na_2C_4O_4$	339	256	3.60	[182]
Na_3PS_3O	379	> 300	4.00	[189]
Na_2O_2	421.5	408	4.00	[187]
AC-Na	316	300	4.10	[188]
$NaCrO_2$	251	229	4.20	[61]
$Na_2C_6O_6$	250	200	3.75	[184]
$Na_4C_6O_6$	412	414	4.00	[183]
$Na_2C_6H_2O_6$	312	302	4.00	[176]
EDTA-4Na	282	420	4.00	[185]
DTPA-5Na	266	363	3.97	[186]

doping, phase mixing, morphological control, surface modification, and sodium compensation. Table 2 compares the electrochemical properties of recently reported P2 layered cathode materials using various modification strategies.

From the table, it should be noted that the simultaneous achievements of high capacity and long cycling stability are still highly challenging. This could be explained by the formidable and interconnected degradation mechanisms that are unlikely to be eliminated by a single or even a combined approach. To develop practical P2 layered oxide materials, we believe that systematic strategies are required with precise understanding on the functionalities from atom to lattice, particle, and electrode. Also, the performances of these reports show huge divergence due to the differences in materials and the testing protocols. For example, using wider electrochemical window can contribute to higher specific capacity. However, this could cause more serious structural/interfacial instability issues that are unacceptable for practical applications. In addition, the manufacturability and cost of the improvement strategies are also critically important in determining their practical applications. While most studies focus on materials engineering, more attention should also be devoted to electrolyte engineering to realize wider electrochemical stability window and dense, stable, and high ionic conductivity electrolyte-electrode interfaces.

In summary, this review has critically examined the progress made in Na-deficient P2-type layered oxide cathodes for SIBs. The inherent advantages and challenges associated with these materials have been discussed, along with promising strategies for improvement through materials and electrode engineering strategies. Continued advancements in materials science, electrode design, and cell engineering hold significant potential to overcome the limitations of P2-type cathodes and expedite their development for practical SIB applications. This study aims to be a valuable resource for researchers and stakeholders working towards realizing high-performance, cost-effective, and sustainable SIBs.

Table 2. Summary of the properties of P2 layered cathode materials using various modification strategies

Materials	Potential range [V *vs.* Na^+/Na]	Discharge capacity [mAh g^{-1}]/I	Energy density [Wh kg^{-1}]	Capacity retention (%)/cycle number	Strategies	Year of publication
$Na_{0.6}[Co_{0.78}Ru_{0.22}]O_2$ [70]	1.5-4.3	163/23.5	499.9	98/50 (1.5-4 V, 23.5)	Compositional design	2023
P2-$Na_{2/3}Mn_xNi_{x-1/3}Co_{4/3-2x}O_2$($1/3 \leq x \leq 2/3$) [77]	1.5-4.5	156/50	410	87/300 (1.5-4.0 V, 1,000)	Compositional design	2021
$Na_{2/3}Li_{1/6}Co_{1/6}Mn_{2/3}O_2$ [82]	2.0-4.5	178/15	534	95.8/250 (150)	Compositional design	2023
$Na_{0.67}Mn_{0.53}Ni_{0.30}Mg_{0.085}Ti_{0.085}O_2$ [83]	2.0-4.25	118/50	410	91.5/100 (50)	Compositional design	2023
$Na_{0.67}(Mn_{0.45}Ni_{0.18}Co_{0.18}Ti_{0.1}Mg_{0.03}Al_{0.04}Fe_{0.02})O_2$ [85]	1.5-4.6	146/20	477	69/50 (100)	Compositional design	2023
$Na_{2/3}[Ni_{1/4}Mn_{1/2}Ti_{1/6}Zn_{1/12}]O_2$ [86]	2.5-4.5	116/13	-	higher (33%) than pristine/40 (13)	Compositional design	2023
$Na_{0.67}Mn_{1-x}Mo_xO_2$ [88]	1.8-4.3	109.73/2,000	-	86.4/100 (50)	Elemental doping	2021
$Na_{0.612}K_{0.056}MnO_2$ [89]	1.0-4.3	240.5/20	654	98.2/100 (50)	Elemental doping	2021
$Na_{0.76}Ca_{0.05}[Ni_{0.230.08}Mn_{0.69}]O_2$ [91]	2.0-4.3	153.9/12	257.6	87.1/50 (12)	Elemental doping	2021
$Na_{0.67}Ni_{0.3}Co_{0.1}Mn_{0.6}O_{1.94}(BO_3)_{0.02}$ [99]	2.0-4.1	98.7/30	-	80.1/1,000 (300)	Elemental doping	2022
$Na_{0.67}Ni_{0.15}Fe_{0.2}Mn_{0.65}F_{0.05}O_{1.95}$ [102]	1.5-4.3	229/0.1C	-	87.7/50 (0.1C)	Elemental doping	2022
$Na_{0.667}Mn_{0.667}Ni_{0.167}Co_{0.117}Ti_{0.01}Mg_{0.01}Cu_{0.01}Mo_{0.01}Nb_{0.01}O_2$ [103]	1.5-4.5	111/875	-	76.4/100 (175)	Elemental doping	2023
P2/O'3-biphasic $NaMn_{0.89}Cu_{0.08}Sb_{0.03}O_2$ [9]	2.0-4.0	204/10	-	80/150 (500)	Phase mixing & Compositional design	2020
P2/Li-O3 $Na_{0.67}Mn_{0.67}Ni_{0.33}O_2$ [106]	2.0-4.5	104/850	-	60/200 (85)	Phase mixing & Elemental doping & Morphological control	2022
P2/O3 biphasic $Na_{0.7}Ni_{0.2}Cu_{0.1}Fe_{0.2}Mn_{0.5}O_{2-\delta}$ [114]	1.5-4.1	62/2,400	190	84/500 (600)	Phase mixing	2022
P2@P3-$Na_{0.5}Ni_{0.1}Co_{0.15}Mn_{0.65}Mg_{0.1}O_2$ [116]	1.5-4.0	153.8/16	325.8	80.6/320 (200)	Phase mixing & Compositional design	2020
layered–tunnel $Na_{0.6}Mn_{0.95}Mg_{0.05}O_{2x}Mg_xO_2$ [120]	2.0-4.0	188.9/100	508	71.3/1,000(1,000)	Phase mixing & Compositional design	2023
P3/P2/O3-$Na_{0.674}Ni_{0.319}Mn_{0.590}O_2$ [124]	2.0-4.2	155.4/15	-	51.5/200 (15)	Phase mixing	2022
$Na_{0.76}Cu_{0.22}Fe_{0.30}Mn_{0.48}O_2$ [127]	2.0-4.0	125.4/12	177.4	79/300 (240)	Morphological control & Elemental doping	2020

P2-$Na_{0.67}Ni_{0.23}Mg_{0.1}Mn_{0.67}O_2$ [130]	2.5-4.35	60/850	249.9	90.9/1,000 (850)	Morphological control & Elemental doping	2021
$Na_{0.6}Mn_{0.95}Ti_{0.05}O_2$ [137]	2.0-4.1	106.4/20	296.1	89.6/100	Morphology & Compositional design	2023
single-crystal P2-type $Na_{0.66}Ni_{0.26}Zn_{0.07}Mn_{0.67}O_2$ [140]	2.0-4.4	122.1/10	-	95.8/100 (100)	Morphological control & Elemental doping	2023
$Na_{0.62}Mn_{0.67}Ni_{0.23}Cu_{0.05}Mg_{0.07}Ti_{0.01}O_2$ [141]	2.0-4.3	78.6/1200	-	87/500 (120)	Morphology & Compositional design	2022
shale-like Na_xMnO_2 [143]	1.5-4.0	181/24	-	83/3,000 (960, 2.0-4.0 V)	Morphology	2021
$Na_{2/3}Ni_{1/3}Mn_{2/3}O_2$ with ZrO_2 coating [149]	2.0-4.5	157.8/87.5	-	86/1,000 (875)	Surface modification & Elemental doping	2022
ZrO_2-$Na_{0.67}Ni_{0.28}Mg_{0.05}Mn_{0.67}O_2$ [150]	2.0-4.35	121.9/12	238.91	81.5/150 (120)	Surface modification & Elemental doping	2023
$CaTiO_3$-$Na_{2/3}Ni_{1/3}Mn_{2/3}O_2$ [151]	1.5-4.5	178/17.3	-	75.3/200 (346)	Surface modification & Elemental doping	2022
$Na_{2/3}Ni_{1/3}Mn_{2/3}O_2$-$Al_2O_3$ ALD [156]	1.5-4.1	200/15	-	87/300 (750)	Surface modification	2021
Al_2O_3@$Na_{0.67}Zn_{0.1}Mn_{0.9}O_2$ [157]	2.0-4.4	156/12		85/400 (120)	Surface modification & Compositional design	2020
alucone coated P2-type $Na_{0.66}Mn_{0.9}Mg_{0.1}O_2$ [158]	2.0-4.5	163.1/200	-	86/100 (200)	Surface modification & Elemental doping	2020

DECLARATIONS

Authors' contributions

Made substantial contributions to the conception and design of the study and provided administrative and technical support: Zhu X, Li K
Performed data acquisition and writing: Huang Y, Zeng W, Zhu X

Availability of data and materials

Not applicable.

Financial support and sponsorship

This work was supported by the National Natural Science Foundation of China (52202210) and the Scientific Research Fund of Hunan Provincial Education Department (22B0292).

Conflicts of interest

The other authors declared that there are no conflicts of interest.
Kui Li and Weixiong Zeng are affiliated with "Tuo Feng New Energy Co., Ltd, China".

Ethical approval and consent to participate

Not applicable.

Consent for publication

Not applicable.

Copyright

REFERENCES

1. Van der Ven A, Deng Z, Banerjee S, Ong SP. Rechargeable alkali-ion battery materials: theory and computation. *Chem Rev* 2020;120:6977-7019. DOI PubMed
2. Larcher D, Tarascon JM. Towards greener and more sustainable batteries for electrical energy storage. *Nat Chem* 2015;7:19-29. DOI PubMed
3. Zhu X, Lin T, Manning E, et al. Recent advances on Fe- and Mn-based cathode materials for lithium and sodium ion batteries. *J Nanopart Res* 2018;20:160. DOI
4. Yabuuchi N, Kajiyama M, Iwatate J, et al. P2-type $Na_x[Fe_{1/2}Mn_{1/2}]O_2$ made from earth-abundant elements for rechargeable Na batteries. *Nat Mater* 2012;11:512-7. DOI
5. Yaroshevsky AA. Abundances of chemical elements in the Earth's crust. *Geochem Int* 2006;44:48-55. DOI
6. USG Survey. Mineral commodity summaries. Available from: https://pubs.usgs.gov/publication/mcs2023 [Last accessed on 11 May 2024].
7. Rudola A, Wright CJ, Barker J. Reviewing the safe shipping of lithium-ion and sodium-ion cells: a materials chemistry perspective. *Energy Mater Adv* 2021;2021:2021/9798460. DOI
8. Zhu X, Wang L. Advances in materials for all-climate sodium-ion batteries. *EcoMat* 2020;2:e12043. DOI
9. Liu Z, Jiang K, Chu S, et al. Integrating P2 into O′3 toward a robust Mn-based layered cathode for sodium-ion batteries. *J Mater Chem A* 2020;8:23820-6. DOI
10. Zhu X, Mochiku T, Fujii H, et al. A new sodium iron phosphate as a stable high-rate cathode material for sodium ion batteries. *Nano Res* 2018;11:6197-205. DOI
11. Liang X, Hwang J, Sun Y. Practical cathodes for sodium-ion batteries: who will take the crown? *Adv Energy Mater* 2023;13:2301975. DOI
12. Delmas C, Carlier D, Guignard M. The layered oxides in lithium and sodium-ion batteries: a solid-state chemistry approach. *Adv Energy Mater* 2021;11:2001201. DOI
13. Peng B, Wan G, Ahmad N, Yu L, Ma X, Zhang G. Recent progress in the emerging modification strategies for layered oxide cathodes toward practicable sodium ion batteries. *Adv Energy Mater* 2023;13:2300334. DOI
14. Zhang Y, Zhang R, Huang Y. Air-stable Na_xTMO_2 cathodes for sodium storage. *Front Chem* 2019;7:335. DOI PubMed PMC
15. Wang X, Zhang Q, Zhao C, et al. Achieving a high-performance sodium-ion pouch cell by regulating intergrowth structures in a layered oxide cathode with anionic redox. *Nat Energy* 2024;9:184-96. DOI
16. Johnston W, Heikes R, Sestrich D. The preparation, crystallography, and magnetic properties of the $LixCo_{1-x}O$ system. *J Phys Chem Solids* 1958;7:1-13. DOI
17. Mizushima K, Jones P, Wiseman P, Goodenough J. Li_xCoO_2 (0<x<-1): a new cathode material for batteries of high energy density. *Mater Res Bull* 1980;15:783-9. DOI
18. Fouassier C, Matejka G, Reau J, Hagenmuller P. Sur de nouveaux bronzes oxygénés de formule $Na\chi CoO_2(\chi 1)$. Le système cobalt-oxygène-sodium. *J Solid State Chem* 1973;6:532-7. DOI
19. Delmas C, Braconnier J, Fouassier C, Hagenmuller P. Electrochemical intercalation of sodium in Na_xCoO_2 bronzes. *Solid State Ion* 1981;3-4:165-9. DOI
20. Braconnier J, Delmas C, Hagenmuller P. Etude par desintercalation electrochimique des systemes Na_xCrO_2 et Na_xNiO_2. *Mater Res Bull* 1982;17:993-1000. DOI
21. Maazaz A, Delmas C, Hagenmuller P. A study of the Na_xTiO_2 system by electrochemical deintercalation. *J Incl Phenom* 1983;1:45-51. DOI
22. Delmas C, Fouassier C, Hagenmuller P. Structural classification and properties of the layered oxides. *Physica B+C* 1980;99:81-5. DOI
23. Katcho NA, Carrasco J, Saurel D, et al. Origins of bistability and na ion mobility difference in P2- and O3-$Na_{2/3}Fe_{2/3}Mn_{1/3}O_2$ cathode

polymorphs. *Adv Energy Mater* 2017;7:1601477. DOI
24. Zhao C, Wang Q, Yao Z, et al. Rational design of layered oxide materials for sodium-ion batteries. *Science* 2020;370:708-11. DOI
25. Kim D, Kang S, Slater M, et al. Enabling sodium batteries using lithium-substituted sodium layered transition metal oxide cathodes. *Adv Energy Mater* 2011;1:333-6. DOI
26. Cheng Z, Zhao B, Guo Y, et al. Mitigating the large-volume phase transition of P2-type cathodes by synergetic effect of multiple ions for improved sodium-ion batteries. *Adv Energy Mater* 2022;12:2103461. DOI
27. Lee DH, Xu J, Meng YS. An advanced cathode for Na-ion batteries with high rate and excellent structural stability. *Phys Chem Chem Phys* 2013;15:3304-12. DOI
28. Jung YH, Christiansen AS, Johnsen RE, Norby P, Kim DK. In situ X-ray diffraction studies on structural changes of a P2 layered material during electrochemical desodiation/sodiation. *Adv Funct Mater* 2015;25:3227-37. DOI
29. Sathiya M, Jacquet Q, Doublet M, Karakulina OM, Hadermann J, Tarascon J. A chemical approach to raise cell voltage and suppress phase transition in O3 sodium layered oxide electrodes. *Adv Energy Mater* 2018;8:1702599. DOI
30. Ong SP, Chevrier VL, Hautier G, et al. Voltage, stability and diffusion barrier differences between sodium-ion and lithium-ion intercalation materials. *Energy Environ Sci* 2011;4:3680-88. DOI
31. Liu Z, Xu X, Ji S, Zeng L, Zhang D, Liu J. Recent progress of P2-type layered transition-metal oxide cathodes for sodium-ion batteries. *Chemistry* 2020;26:7747-66. DOI
32. Paidi AK, Park WB, Ramakrishnan P, et al. Unravelling the nature of the intrinsic complex structure of binary-phase Na-layered oxides. *Adv Mater* 2022;34:e2202137. DOI
33. Jung R, Morasch R, Karayaylali P, et al. Effect of ambient storage on the degradation of Ni-rich positive electrode materials (NMC811) for Li-Ion batteries. *J Electrochem Soc* 2018;165:A132-41. DOI
34. You Y, Dolocan A, Li W, Manthiram A. Understanding the air-exposure degradation chemistry at a nanoscale of layered oxide cathodes for sodium-Ion batteries. *Nano Lett* 2019;19:182-8. DOI
35. Zheng L, Li L, Shunmugasundaram R, Obrovac MN. Effect of controlled-atmosphere storage and ethanol rinsing on $NaNi_{0.5}Mn_{0.5}O_2$ for sodium-ion batteries. *ACS Appl Mater Interfaces* 2018;10:38246-54. DOI
36. Sun Y, Wang H, Meng D, et al. Degradation mechanism of O3-type $NaNi_{1/3}Fe_{1/3}Mn_{1/3}O_2$ cathode materials during ambient storage and their in situ regeneration. *ACS Appl Energy Mater* 2021;4:2061-7. DOI
37. Zuo W, Qiu J, Liu X, et al. The stability of P2-layered sodium transition metal oxides in ambient atmospheres. *Nat Commun* 2020;11:3544. DOI PubMed PMC
38. Mu L, Hou Q, Yang Z, et al. Water-processable P2-$Na_{0.67}Ni_{0.22}Cu_{0.11}Mn_{0.56}Ti_{0.11}O_2$ cathode material for sodium ion batteries. *J Electrochem Soc* 2019;166:A251-7. DOI
39. Han MH, Gonzalo E, Sharma N, et al. High-performance P2-phase $Na_{2/3}Mn_{0.8}Fe_{0.1}Ti_{0.1}O_2$ cathode material for ambient-temperature sodium-ion batteries. *Chem Mater* 2016;28:106-16. DOI
40. Deng Y, Wu Z, Liang R, et al. Layer-based heterostructured cathodes for lithium-ion and sodium-ion batteries. *Adv Funct Mater* 2019;29:1808522. DOI
41. Song T, Kendrick E. Recent progress on strategies to improve the high-voltage stability of layered-oxide cathode materials for sodium-ion batteries. *J Phys Mater* 2021;4:032004. DOI
42. Hwang J, Kim J, Yu T, Sun Y. A new P2-type layered oxide cathode with extremely high energy density for sodium-ion batteries. *Adv Energy Mater* 2019;9:1803346. DOI
43. Lu Z, Dahn JR. In situ X-ray diffraction study of P2-$Na_{2/3}[Ni_{1/3}Mn_{2/3}]O_2$. *J Electrochem Soc* 2001;148:A1225. DOI
44. Yang L, Li X, Liu J, et al. Lithium-doping stabilized high-performance P2-$Na_{0.66}Li_{0.18}Fe_{0.12}Mn_{0.7}O_2$ cathode for sodium ion batteries. *J Am Chem Soc* 2019;141:6680-9. DOI
45. Singh G, Tapia-ruiz N, Lopez del Amo JM, et al. High voltage Mg-doped $Na_{0.67}Ni_{0.3-x}Mg_xMn_{0.7}O_2$ (x = 0.05, 0.1) Na-Ion cathodes with enhanced stability and rate capability. *Chem Mater* 2016;28:5087-94. DOI
46. Yuan D, Hu X, Qian J, et al. P2-type $Na_{0.67}Mn_{0.65}Fe_{0.2}Ni_{0.15}O_2$ cathode material with high-capacity for sodium-ion battery. *Electrochim Acta* 2014;116:300-5. DOI
47. Jiang M, Qian G, Liao X, et al. Revisiting the capacity-fading mechanism of P2-type sodium layered oxide cathode materials during high-voltage cycling. *J Energy Chem* 2022;69:16-25. DOI
48. Martens I, Vostrov N, Mirolo M, et al. Defects and nanostrain gradients control phase transition mechanisms in single crystal high-voltage lithium spinel. *Nat Commun* 2023;14:6975. DOI PubMed PMC
49. Martens I, Vostrov N, Mirolo M, et al. Revisiting phase transformation mechanisms in $LiNi_{0.5}Mn_{1.5}O_4$ high voltage cathodes with operando microdiffraction. *ACS Mater Lett* 2022;4:2528-36. DOI
50. Asl HY, Manthiram A. Reining in dissolved transition-metal ions. *Science* 2020;369:140-1. DOI PubMed
51. Zhu X, Sun D, Luo B, Hu Y, Wang L. A stable high-power $Na_2Ti_3O_7$/$LiNi_{0.5}Mn_{1.5}O_4$ Li-ion hybrid energy storage device. *Electrochim Acta* 2018;284:30-7. DOI
52. Lu Z, Dahn JR. Intercalation of water in P2, T2 and O2 structure $A_z[Co_xNi_{1/3-x}Mn_{2/3}]O_2$. *Chem Mater* 2001;13:1252-7. DOI
53. Duffort V, Talaie E, Black R, Nazar LF. Uptake of CO_2 in layered P2-$Na_{0.67}Mn_{0.5}Fe_{0.5}O_2$: insertion of carbonate anions. *Chem Mater* 2015;27:2515-24. DOI
54. Tang J, Kye DK, Pol VG. Ultrasound-assisted synthesis of sodium powder as electrode additive to improve cycling performance of sodium-ion batteries. *J Power Sources* 2018;396:476-82. DOI

55. Xiao B, Soto FA, Gu M, et al. Lithium-pretreated hard carbon as high-performance sodium-ion battery anodes. *Adv Energy Mater* 2018;8:1801441. DOI
56. Zhang B, Dugas R, Rousse G, Rozier P, Abakumov AM, Tarascon JM. Insertion compounds and composites made by ball milling for advanced sodium-ion batteries. *Nat Commun* 2016;7:10308. DOI PubMed PMC
57. Park K, Yu B, Goodenough JB. Electrochemical and chemical properties of Na_2NiO_2 as a cathode additive for a rechargeable sodium battery. *Chem Mater* 2015;27:6682-8. DOI
58. Jo C, Choi JU, Yashiro H, Myung S. Controllable charge capacity using a black additive for high-energy-density sodium-ion batteries. *J Mater Chem A* 2019;7:3903-9. DOI
59. Sathiya M, Thomas J, Batuk D, Pimenta V, Gopalan R, Tarascon J. Dual stabilization and sacrificial effect of Na_2CO_3 for increasing capacities of Na-Ion cells based on P2-Na_xMO_2 electrodes. *Chem Mater* 2017;29:5948-56. DOI
60. Singh G, Acebedo B, Cabanas MC, Shanmukaraj D, Armand M, Rojo T. An approach to overcome first cycle irreversible capacity in P2-$Na_{2/3}[Fe_{1/2}Mn_{1/2}]O_2$. *Electrochem Commun* 2013;37:61-3. DOI
61. Shen B, Zhan R, Dai C, et al. Manipulating irreversible phase transition of $NaCrO_2$ towards an effective sodium compensation additive for superior sodium-ion full cells. *J Colloid Interface Sci* 2019;553:524-9. DOI
62. Martinez De Ilarduya J, Otaegui L, López del Amo JM, Armand M, Singh G. NaN_3 addition, a strategy to overcome the problem of sodium deficiency in P2-$Na_{0.67}[Fe_{0.5}Mn_{0.5}]O_2$ cathode for sodium-ion battery. *J Power Sources* 2017;337:197-203. DOI
63. Niu Y, Guo Y, Yin Y, et al. High-efficiency cathode sodium compensation for sodium-ion batteries. *Adv Mater* 2020;32:2001419. DOI
64. Shacklette LW, Jow TR, Townsend L. Rechargeable electrodes from sodium cobalt bronzes. *J Electrochem Soc* 1988;135:2669-74. DOI
65. Mendiboure A, Delmas C, Hagenmuller P. Electrochemical intercalation and deintercalation of Na_xMnO_2 bronzes. *J Solid State Chem* 1985;57:323-31. DOI
66. Hamani D, Ati M, Tarascon J, Rozier P. Na_xVO_2 as possible electrode for Na-ion batteries. *Electrochem Commun* 2011;13:938-41. DOI
67. Berthelot R, Carlier D, Delmas C. Electrochemical investigation of the P2-Na_xCoO_2 phase diagram. *Nat Mater* 2011;10:74-80. DOI PubMed
68. Caballero A, Hernán L, Morales J, Sánchez L, Santos Peña J, Aranda MAG. Synthesis and characterization of high-temperature hexagonal P2-$Na_{0.6}MnO_2$ and its electrochemical behaviour as cathode in sodium cells. *J Mater Chem* 2002;12:1142-7. DOI
69. Wang Y, Shadike Z, Fitzhugh W, et al. Tuning discharge voltage by Schottky electron barrier in P2-$Na_{2/3}Mg_{0.205}Ni_{0.1}Fe_{0.05}Mn_{0.645}O_2$. *Energy Stor Mater* 2023;55:587-96. DOI
70. Voronina N, Köster K, Yu JH, et al. Unveiling the role of ruthenium in layered sodium cobaltite toward high-performance electrode enabled by anionic and cationic redox. *Adv Energy Mater* 2023;13:2302017. DOI
71. She Q, Xu J, Huang A, et al. Limiting cobalt fraction in lithium rich cathode materials for stable and fast activation. *Chem Eng Sci* 2024;284:119526. DOI
72. Zhang J, Wang W, Wang W, Wang S, Li B. Comprehensive review of P2-type $Na_{2/3}Ni_{1/3}Mn_{2/3}O_2$, a potential cathode for practical application of Na-ion batteries. *ACS Appl Mater Interfaces* 2019;11:22051-66. DOI
73. Lu Z, Donaberger RA, Dahn JR. Superlattice ordering of Mn, Ni, and Co in layered alkali transition metal oxides with P2, P3, and O3 Structures. *Chem Mater* 2000;12:3583-90. DOI
74. Zhang Y, Wu M, Ma J, et al. Revisiting the $Na_{2/3}Ni_{1/3}Mn_{2/3}O_2$ cathode: oxygen redox chemistry and oxygen release suppression. *ACS Cent Sci* 2020;6:232-40. DOI PubMed PMC
75. Liu L, Li X, Bo S, et al. High-performance P2-type $Na_{2/3}(Mn_{1/2}Fe_{1/4}Co_{1/4})O_2$ cathode material with superior rate capability for Na-ion batteries. *Adv Energy Mater* 2015;5:1500944. DOI
76. Li Z, Gao R, Sun L, Hu Z, Liu X. Designing an advanced P2-$Na_{0.67}Mn_{0.65}Ni_{0.2}Co_{0.15}O_2$ layered cathode material for Na-ion batteries. *J Mater Chem A* 2015;3:16272-8. DOI
77. Liu Z, Shen J, Feng S, et al. Ultralow volume change of P2-type layered oxide cathode for Na-ion batteries with controlled phase transition by regulating distribution of Na. *Angew Chem Int Ed* 2021;60:20960-9. DOI
78. Wang PF, Yao HR, Liu XY, et al. Na^+/vacancy disordering promises high-rate Na-ion batteries. *Sci Adv* 2018;4:eaar6018. DOI PubMed PMC
79. Tang K, Huang Y, Xie X, et al. Electrochemical performance and structural stability of air-stable $Na_{0.67}Ni_{0.33}Mn_{0.67-x}Ti_xO_2$ cathode materials for high-performance sodium-ion batteries. *Chem Eng J* 2020;399:125725. DOI
80. Wang Y, Wang Y, Xing Y, et al. Entropy modulation strategy of P2-type layered transition metal oxide cathodes for sodium-ion batteries with a high performance. *J Mater Chem A* 2023;11:19955-64. DOI
81. Yoshida H, Yabuuchi N, Kubota K, et al. P2-type $Na_{2/3}Ni_{1/3}Mn_{2/3-x}Ti_xO_2$ as a new positive electrode for higher energy Na-ion batteries. *Chem Commun* 2014;50:3677-80. DOI PubMed
82. Zou P, Yao L, Wang C, Lee SJ, Li T, Xin HL. Regulating cation interactions for zero-strain and high-voltage P2-type $Na_{2/3}Li_{1/6}Co_{1/6}Mn_{2/3}O_2$ layered oxide cathodes of sodium-ion batteries. *Angew Chem Int Ed* 2023;62:e202304628. DOI
83. Liu Z, Wu J, Zeng J, et al. Co-free layered oxide cathode material with stable anionic redox reaction for sodium-ion batteries. *Adv Energy Mater* 2023;13:2301471. DOI
84. Dreyer SL, Zhang R, Wang J, et al. The effect of configurational entropy on acoustic emission of P2-type layered oxide cathodes for

sodium-ion batteries. *J Phys Energy* 2023;5:035002. DOI

85. Wang J, Dreyer SL, Wang K, et al. P2-type layered high-entropy oxides as sodium-ion cathode materials. *Mater Futures* 2022;1:035104. DOI
86. Kubota K, Asari T, Komaba S. Impact of Ti and Zn dual-substitution in P2 type $Na_{2/3}Ni_{1/3}Mn_{2/3}O_2$ on Ni-Mn and Na-vacancy ordering and electrochemical properties. *Adv Mater* 2023;35:e2300714. DOI
87. Li Y, Chen M, Liu B, Zhang Y, Liang X, Xia X. Heteroatom doping: an effective way to boost sodium ion storage. *Adv Energy Mater* 2020;10:2000927. DOI
88. Zhang L, Wang C, Liu Y, et al. Suppressing interlayer-gliding and Jahn-teller effect in P2-type layered manganese oxide cathode via Mo doping for sodium-ion batteries. *Chem Eng J* 2021;426:130813. DOI
89. Wang C, Liu L, Zhao S, et al. Tuning local chemistry of P2 layered-oxide cathode for high energy and long cycles of sodium-ion battery. *Nat Commun* 2021;12:2256. DOI PubMed PMC
90. Ma C, Alvarado J, Xu J, et al. Exploring oxygen activity in the high energy P2-type $Na_{0.78}Ni_{0.23}Mn_{0.69}O_2$ cathode material for Na-ion batteries. *J Am Chem Soc* 2017;139:4835-45. DOI
91. Shen Q, Liu Y, Zhao X, et al. Transition-metal vacancy manufacturing and sodium-site doping enable a high-performance layered oxide cathode through cationic and anionic redox chemistry. *Adv Funct Mater* 2021;31:2106923. DOI
92. Fu H, Wang YP, Fan G, et al. Synergetic stability enhancement with magnesium and calcium ion substitution for Ni/Mn-based P2-type sodium-ion battery cathodes. *Chem Sci* 2022;13:726-36. DOI PubMed PMC
93. Li C, Geng F, Hu B, Hu B. Anionic redox in Na-based layered oxide cathodes: a review with focus on mechanism studies. *Mater Today Energy* 2020;17:100474. DOI
94. Huang Z, Gu Z, Heng Y, Huixiang Ang E, Geng H, Wu X. Advanced layered oxide cathodes for sodium/potassium-ion batteries: development, challenges and prospects. *Chem Eng J* 2023;452:139438. DOI
95. Wang X, Yin L, Ronne A, et al. Stabilizing lattice oxygen redox in layered sodium transition metal oxide through spin singlet state. *Nat Commun* 2023;14:7665. DOI PubMed PMC
96. Wang T, Ren GX, Xia HY, et al. Anionic redox regulated via metal-ligand combinations in layered sulfides. *Adv Mater* 2022;34:e2107353. DOI
97. Cai C, Li X, Hu P, et al. Comprehensively strengthened metal-oxygen bonds for reversible anionic redox reaction. *Adv Funct Mater* 2023;33:2215155. DOI
98. Liu K, Tan S, Moon J, et al. Insights into the enhanced cycle and rate performances of the F-substituted P2-type oxide cathodes for sodium-ion batteries. *Adv Energy Mater* 2020;10:2000135. DOI
99. Wang X, Dong X, Feng X, et al. In-plane BO_3 configuration in P2 layered oxide enables outstanding long cycle performance for sodium ion batteries. *Small Methods* 2023;7:e2201201. DOI
100. Chae MS, Kim HJ, Lyoo J, et al. Anomalous sodium storage behavior in Al/F dual-doped P2-type sodium manganese oxide cathode for sodium-ion batteries. *Adv Energy Mater* 2020;10:2002205. DOI
101. Mao Q, Yu Y, Wang J, et al. Mitigating the P2-O_2 transition and Na^+/vacancy ordering in $Na_{2/3}Ni_{1/3}Mn_{2/3}O_2$ by anion/cation dual-doping for fast and stable Na^+ insertion/extraction. *J Mater Chem A* 2021;9:10803-11. DOI
102. Cui X, Wang S, Ye X, et al. Insights into the improved cycle and rate performance by ex-situ F and in-situ Mg dual doping of layered oxide cathodes for sodium-ion batteries. *Energy Stor Mater* 2022;45:1153-64. DOI
103. Ma S, Zou P, Xin HL. Extending phase-variation voltage zones in P2-type sodium cathodes through high-entropy doping for enhanced cycling stability and rate capability. *Mater Today Energy* 2023;38:101446. DOI
104. Lee E, Lu J, Ren Y, et al. Layered P2/O_3 intergrowth cathode: toward high power Na-ion batteries. *Adv Energy Mater* 2014;4:1400458. DOI
105. Guo S, Liu P, Yu H, et al. A layered P2- and O3-type composite as a high-energy cathode for rechargeable sodium-ion batteries. *Angew Chem Int Ed* 2015;54:5894-9. DOI
106. Huang Q, Wang M, Zhang L, et al. Shear-resistant interface of layered oxide cathodes for sodium ion batteries. *Energy Stor Mater* 2022;45:389-98. DOI
107. Li Z, Zhang J, Gao R, et al. Li-substituted co-free layered P2/O3 biphasic $Na_{0.67}Mn_{0.55}Ni_{0.25}Ti_{0.2-x}Li_xO_2$ as high-rate-capability cathode materials for sodium ion batteries. *J Phys Chem C* 2016;120:9007-16. DOI
108. Zhou D, Huang W, Lv X, Zhao F. A novel P2/O3 biphase $Na_{0.67}Fe_{0.425}Mn_{0.425}Mg_{0.15}O_2$ as cathode for high-performance sodium-ion batteries. *J Power Sources* 2019;421:147-55. DOI
109. Yu L, Cheng Z, Xu K, et al. Interlocking biphasic chemistry for high-voltage P2/O3 sodium layered oxide cathode. *Energy Stor Mater* 2022;50:730-9. DOI
110. Chen C, Huang W, Li Y, et al. P2/O3 biphasic Fe/Mn-based layered oxide cathode with ultrahigh capacity and great cyclability for sodium ion batteries. *Nano Energy* 2021;90:106504. DOI
111. Liang X, Sun Y. A novel pentanary metal oxide cathode with P2/O3 biphasic structure for high-performance sodium-ion batteries. *Adv Funct Mater* 2022;32:2206154. DOI
112. Zhou P, Che Z, Liu J, et al. High-entropy P2/O3 biphasic cathode materials for wide-temperature rechargeable sodium-ion batteries. *Energy Stor Mater* 2023;57:618-27. DOI
113. Mu J, Cai T, Dong W, Zhou C, Han Z, Huang F. Biphasic high-entropy layered oxide as a stable and high-rate cathode for sodium-ion batteries. *Chem Eng J* 2023;471:144403. DOI

114. Gao X, Liu H, Chen H, et al. Cationic-potential tuned biphasic layered cathodes for stable desodiation/sodiation. *Sci Bull* 2022;67:1589-602. DOI
115. Lin C, Dai P, Wang X, et al. P2/O3 biphase integration promoting the enhancement of structural stability for sodium layered oxide cathode. *Chem Eng J* 2024;480:147964. DOI
116. Zhu YF, Xiao Y, Hua WB, et al. Manipulating layered P2@P3 integrated spinel structure evolution for high-performance sodium-ion batteries. *Angew Chem Int Ed* 2020;59:9299-304. DOI
117. Wu ZG, Li JT, Zhong YJ, et al. Mn-based cathode with synergetic layered-tunnel hybrid structures and their enhanced electrochemical performance in sodium ion batteries. *ACS Appl Mater Interfaces* 2017;9:21267-75. DOI PubMed
118. Xiao Y, Wang P, Yin Y, et al. A layered-tunnel intergrowth structure for high-performance sodium-ion oxide cathode. *Adv Energy Mater* 2018;8:1800492. DOI
119. Huang Q, Feng Y, Xu S, et al. A P2@tunnel heterostructure cathode for high-performance sodium-ion batteries. *ChemElectroChem* 2020;7:4383-9. DOI
120. Xiao Y, Liu Y, Li H, et al. Insights into layered-tunnel dynamic structural evolution based on local coordination chemistry regulation for high-energy-density and long-cycle-life sodium-ion oxide cathodes. *InfoMat* 2023;5:e12475. DOI
121. Gao G, Tie D, Ma H, et al. Interface-rich mixed P2+T phase $Na_xCo_{0.1}Mn_{0.9}O_2(0.44 \leq x \leq 0.7)$ toward fast and high capacity sodium storage. *J Mater Chem A* 2018;6:6675-84. DOI
122. Feng J, Yang Z, Zhong J, Zheng C, Wei Z, Li J. Integrating superlattice to regulate P2-O2 phase transition and improve cycling stability in sodium-ion batteries. *Batteries Supercaps* 2022;5:e202200115. DOI
123. Vanam SP, Barpanda P. A molybdenum doped layer-spinel composite cathode material for sodium-ion battery. *Electrochim Acta* 2022;431:141122. DOI
124. Li R, Gao J, Li J, et al. An undoped tri-phase coexistent cathode material for sodium-ion batteries. *Adv Funct Mater* 2022;32:2205661. DOI
125. Tong Z, Ye Q, Deng Y, et al. Tuning the structural disordering in hierarchical $LiNi_{0.5}Mn_{1.5}O_4$ microrods for stable high-rate electrode performance. *J Alloy Compd* 2023;937:168544. DOI
126. Jung E, Park Y, Park K, et al. Synthesis of nanostructured P2-$Na_{2/3}MnO_2$ for high performance sodium-ion batteries. *Chem Commun* 2019;55:4757-60. DOI PubMed
127. Shen Q, Zhao X, Liu Y, et al. Dual-strategy of cation-doping and nanoengineering enables fast and stable sodium-ion storage in a novel Fe/Mn-based layered oxide cathode. *Adv Sci* 2020;7:2002199. DOI PubMed PMC
128. Zhu X, Li X, Zhu Y, Jin S, Wang Y, Qian Y. $LiNi_{0.5}Mn_{1.5}O_4$ nanostructures with two-phase intergrowth as enhanced cathodes for lithium-ion batteries. *Electrochim Acta* 2014;121:253-7. DOI
129. Liu Y, Shen Q, Zhao X, et al. Hierarchical engineering of porous P2-$Na_{2/3}Ni_{1/3}Mn_{2/3}O_2$ nanofibers assembled by nanoparticles enables superior sodium-ion storage cathodes. *Adv Funct Mater* 2020;30:1907837. DOI
130. Peng B, Sun Z, Zhao L, Li J, Zhang G. Dual-manipulation on P2-$Na_{0.67}Ni_{0.33}Mn_{0.67}O_2$ layered cathode toward sodium-ion full cell with record operating voltage beyond 3.5 V. *Energy Stor Mater* 2021;35:620-9. DOI
131. Zhu X, Li X, Zhu Y, Jin S, Wang Y, Qian Y. Porous $LiNi_{0.5}Mn_{1.5}O_4$ microspheres with different pore conditions: preparation and application as cathode materials for lithium-ion batteries. *J Power Sources* 2014;261:93-100. DOI
132. Zhu X, Luo B, Butburee T, Zhu J, Han S, Wang L. Hierarchical macro/mesoporous NiO as stable and fast-charging anode materials for lithium-ion batteries. *Micropor Mesopor Mat* 2017;238:78-83. DOI
133. Xie M, Li D, He X, et al. Nitrogen-doped meso-macroporous carbon from waste asphalt as high-performance anode materials for alkali-ion batteries. *Sustain Mater Techno* 2023;35:e00535. DOI
134. Chen C, Han Z, Chen S, et al. Core-shell layered oxide cathode for high-performance sodium-ion batteries. *ACS Appl Mater Interfaces* 2020;12:7144-52. DOI
135. Bao S, Luo S, Wang Z, Yan S, Wang Q, Li J. Novel P2-type concentration-gradient $Na_{0.67}Ni_{0.167}Co_{0.167}Mn_{0.67}O_2$ modified by Mn-rich surface as cathode material for sodium ion batteries. *J Power Sources* 2018;396:404-11. DOI
136. Hou P, Dong M, Sun Z, Li F. Compositionally graded high-voltage P2-type cathode with superior structural stability and redox kinetics for advanced Na-ion batteries. *Nano Res* 2024;17:2755-62. DOI
137. Wang D, Deng Y, Liu Y, et al. Sodium-ion batteries towards practical application through gradient Mn-based layer-tunnel cathode. *Nano Energy* 2023;110:108340. DOI
138. Fu H, Li J, Wang L, Yang X, Li X, Lü W. Na-rich layered transition metal oxides with core/shell structures for improved performance of sodium-ion batteries. *J Phys Chem C* 2022;126:20196-203. DOI
139. Pamidi V, Trivedi S, Behara S, Fichtner M, Reddy MA. Micron-sized single-crystal cathodes for sodium-ion batteries. *iScience* 2022;25:104205. DOI PubMed PMC
140. Zhang F, Lu Y, Guo Y, et al. Highly stabilized single-crystal P2-type layered oxides obtained via rational crystal orientation modulation for sodium-ion batteries. *Chem Eng J* 2023;458:141515. DOI
141. Fu F, Liu X, Fu X, et al. Entropy and crystal-facet modulation of P2-type layered cathodes for long-lasting sodium-based batteries. *Nat Commun* 2022;13:2826. DOI PubMed PMC
142. Zhu X, She Q, Wang M, et al. Synchronous densification and conductivity modulation of nano-titanate for pseudocapacitive Li-ion storage. *Adv Funct Mater* 2024;34:2311025. DOI
143. Zuo W, Liu X, Qiu J, et al. Engineering Na^+-layer spacings to stabilize Mn-based layered cathodes for sodium-ion batteries. *Nat*

Commun 2021;12:4903. DOI PubMed PMC
144. Zhu X, Schulli T, Wang L. Stabilizing high-voltage cathode materials for next-generation Li-ion batteries. *Chem Res Chin Univ* 2020;36:24-32. DOI
145. Wang K, Zhang Z, Ding Y, et al. Surface facet dependent cycling stability of layered cathodes. *Adv Funct Mater* 2023;33:2302023. DOI
146. Shi C, Wang L, Chen X, et al. Challenges of layer-structured cathodes for sodium-ion batteries. *Nanoscale Horiz* 2022;7:338-51. DOI
147. Liu Y, Fang X, Zhang A, et al. Layered P2-$Na_{2/3}[Ni_{1/3}Mn_{2/3}]O_2$ as high-voltage cathode for sodium-ion batteries: The capacity decay mechanism and Al_2O_3 surface modification. *Nano Energy* 2016;27:27-34. DOI
148. Shi Y, Li S, Gao A, et al. Probing the structural transition kinetics and charge compensation of the P2-$Na_{0.78}Al_{0.05}Ni_{0.33}Mn_{0.60}O_2$ cathode for sodium ion batteries. *ACS Appl Mater Interfaces* 2019;11:24122-31. DOI
149. Ren H, Zheng L, Li Y, et al. Impurity-vibrational entropy enables quasi-zero-strain layered oxide cathodes for high-voltage sodium-ion batteries. *Nano Energy* 2022;103:107765. DOI
150. Wan G, Peng B, Zhao L, et al. Dual-strategy modification on P2-$Na_{0.67}Ni_{0.33}Mn_{0.67}O_2$ realizes stable high-voltage cathode and high energy density full cell for sodium-ion batteries. *SusMat* 2023;3:58-71. DOI
151. Xia X, Liu T, Cheng C, et al. Suppressing the dynamic oxygen evolution of sodium layered cathodes through synergistic surface dielectric polarization and bulk site-selective co-doping. *Adv Mater* 2023;35:e2209556. DOI
152. Zhu X, Schülli TU, Yang X, et al. Epitaxial growth of an atom-thin layer on a $LiNi_{0.5}Mn_{1.5}O_4$ cathode for stable Li-ion battery cycling. *Nat Commun* 2022;13:1565. DOI PubMed PMC
153. Meng X, Yang XQ, Sun X. Emerging applications of atomic layer deposition for lithium-ion battery studies. *Adv Mater* 2012;24:3589-615. DOI PubMed
154. Tiwari VK, Singh RK. Nanostructured coating strategies of cathode for improved sodium ion battery performance. *Chem Eng J* 2023;471:144592. DOI
155. Alvarado J, Ma C, Wang S, Nguyen K, Kodur M, Meng YS. Improvement of the cathode electrolyte interphase on P2-$Na_{2/3}Ni_{1/3}Mn_{2/3}O_2$ by atomic layer deposition. *ACS Appl Mater Interfaces* 2017;9:26518-30. DOI
156. Ji H, Zhai J, Chen G, et al. Surface engineering suppresses the failure of biphasic sodium layered cathode for high performance sodium-ion batteries. *Adv Funct Mater* 2022;32:2109319. DOI
157. Zuo W, Qiu J, Liu X, et al. Highly-stable P2-$Na_{0.67}MnO_2$ electrode enabled by lattice tailoring and surface engineering. *Energy Stor Mater* 2020;26:503-12. DOI
158. Kaliyappan K, Or T, Deng Y, Hu Y, Bai Z, Chen Z. Constructing safe and durable high-voltage P2 layered cathodes for sodium ion batteries enabled by molecular layer deposition of alucone. *Adv Funct Mater* 2020;30:1910251. DOI
159. Xia J, Wu W, Fang K, Wu X. Enhancing the interfacial stability of P2-type cathodes by polydopamine-derived carbon coating for achieving performance improvement. *Carbon* 2020;157:693-702. DOI
160. Liu Y, Yang J, Guo B, et al. Enhanced electrochemical performance of $Na_{0.5}Ni_{0.25}Mn_{0.75}O_2$ micro-sheets at 3.8 V for Na-ion batteries with nanosized-thin AlF_3 coating. *Nanoscale* 2018;10:12625-30. DOI PubMed
161. Zhang Y, Pei Y, Liu W, et al. $AlPO_4$-coated P2-type hexagonal $Na_{0.7}MnO_{2.05}$ as high stability cathode for sodium ion battery. *Chem Eng J* 2020;382:122697. DOI
162. Jiao J, Wu K, Dang R, et al. A collaborative strategy with ionic conductive Na_2SiO_3 coating and Si doping of P2-$Na_{0.67}Fe_{0.5}Mn_{0.5}O_2$ cathode: an effective solution to capacity attenuation. *Electrochim Acta* 2021;384:138362. DOI
163. Shao Y, Wang X, Li B, et al. Functional surface modification of P2-type layered Mn-based oxide cathode by thin layer of NASICON for sodium-ion batteries. *Electrochim Acta* 2023;442:141915. DOI
164. Li H, Wang T, Wang X, et al. Sodium superionic conductor $NaTi_2(PO_4)_3$ surface layer modified P2-type $Na_{2/3}Ni_{1/3}Mn_{2/3}O_2$ as high-performance cathode for sodium-ion batteries. *J Power Sources* 2021;494:229771. DOI
165. Deng Q, Zheng F, Zhong W, et al. Nanoscale surface modification of P2-type $Na_{0.65}[Mn_{0.70}Ni_{0.16}Co_{0.14}]O_2$ cathode material for high-performance sodium-ion batteries. *Chem Eng J* 2021;404:126446. DOI
166. Lu D, Yao Z, Zhong Y, et al. Polypyrrole-coated sodium manganate hollow microspheres as a superior cathode for sodium ion batteries. *ACS Appl Mater Interfaces* 2019;11:15630-7. DOI
167. Lin J, Huang Q, Dai K, et al. Mitigating interfacial instability of high-voltage sodium layered oxide cathodes with coordinative polymeric structure. *J Power Sources* 2022;552:232235. DOI
168. Niu YB, Yin YX, Guo YG. Nonaqueous sodium-ion full cells: status, strategies, and prospects. *Small* 2019;15:e1900233. DOI PubMed
169. He H, Sun D, Tang Y, Wang H, Shao M. Understanding and improving the initial coulombic efficiency of high-capacity anode materials for practical sodium ion batteries. *Energy Stor Mater* 2019;23:233-51. DOI
170. Zou K, Deng W, Cai P, et al. Prelithiation/presodiation techniques for advanced electrochemical energy storage systems: concepts, applications, and perspectives. *Adv Funct Mater* 2021;31:2005581. DOI
171. Zhao C, Yao Z, Wang Q, et al. Revealing high Na-content P2-type layered oxides as advanced sodium-ion cathodes. *J Am Chem Soc* 2020;142:5742-50. DOI
172. Charrad G, Harmel J, Berthelot R, Taberna P, Simon P, Rozier P. On the synthesis and potential benefit of Na-rich P-type layered oxides for high power Na-ion batteries. *J Solid State Chem* 2023;326:124190. DOI

173. Jin T, Wang PF, Wang QC, et al. Realizing complete solid-solution reaction in high sodium content P2-type cathode for high-performance sodium-ion batteries. *Angew Chem Int Ed* 2020;59:14511-6. DOI
174. Yang X, Wang S, Li H, et al. Boosting the ultrastable high-Na-content P2-type layered cathode materials with zero-strain cation storage via a lithium dual-site substitution approach. *ACS Nano* 2023;17:18616-28. DOI
175. Kumar BS, Kumar R, Pradeep A, et al. Fundamental principles toward designing high Na-containing P2-structured "layered" Na-transition metal oxides as high-performance cathode materials for Na-ion batteries. *Chem Mater* 2022;34:10470-83. DOI
176. Zhang R, Tang Z, Sun D, et al. Sodium citrate as a self-sacrificial sodium compensation additive for sodium-ion batteries. *Chem Commun* 2021;57:4243-6. DOI
177. Zhang Q, Gao X, Shi Y, et al. Electrocatalytic-driven compensation for sodium ion pouch cell with high energy density and long lifespan. *Energy Stor Mater* 2021;39:54-9. DOI
178. Wang H, Xiao Y, Sun C, Lai C, Ai X. A type of sodium-ion full-cell with a layered $NaNi_{0.5}Ti_{0.5}O_2$ cathode and a pre-sodiated hard carbon anode. *RSC Adv* 2015;5:106519-22. DOI
179. Dewar D, Glushenkov AM. Optimisation of sodium-based energy storage cells using pre-sodiation: a perspective on the emerging field. *Energy Environ Sci* 2021;14:1380-401. DOI
180. Hwang J, Myung S, Lee J, Abouimrane A, Belharouak I, Sun Y. Ultrafast sodium storage in anatase TiO_2 nanoparticles embedded on carbon nanotubes. *Nano Energy* 2015;16:218-26. DOI
181. Sathiya M, Thomas J, Batuk D, Pimenta V, Gopalan R, Tarascon J. Dual stabilization and sacrificial effect of Na_2CO_3 for increasing capacities of Na-ion cells based on P2-Na_xMO_2 electrodes. *Chem Mater* 2017;29:5948-56. DOI
182. Shanmukaraj D, Kretschmer K, Sahu T, et al. Highly efficient, cost effective, and safe sodiation agent for high-performance sodium-ion batteries. *ChemSusChem* 2018;11:3286-91. DOI
183. Zhang Z, Zhang R, Rajagopalan R, et al. A high-capacity self-sacrificial additive based on electroactive sodiated carbonyl groups for sodium-ion batteries. *Chem Commun* 2022;58:8702-5. DOI
184. Marelli E, Marino C, Bolli C, Villevieille C. How to overcome Na deficiency in full cell using P2-phase sodium cathode-a proof of concept study of Na-rhodizonate used as sodium reservoir. *J Power Sources* 2020;450:227617. DOI
185. Jo JH, Choi JU, Park YJ, Zhu J, Yashiro H, Myung ST. New insight into ethylenediaminetetraacetic acid tetrasodium salt as a sacrificing sodium ion source for sodium-deficient cathode materials for full cells. *ACS Appl Mater Interfaces* 2019;11:5957-65. DOI PubMed
186. Jo JH, Choi JU, Park YJ, Ko JK, Yashiro H, Myung S. A new pre-sodiation additive for sodium-ion batteries. *Energy Stor Mater* 2020;32:281-9. DOI
187. Guo YJ, Niu YB, Wei Z, et al. Insights on electrochemical behaviors of sodium peroxide as a sacrificial cathode additive for boosting energy density of Na-ion battery. *ACS Appl Mater Interfaces* 2021;13:2772-8. DOI
188. Zhang T, Kong J, Shen C, et al. Converting residual alkali into sodium compensation additive for high-energy Na-ion batteries. *ACS Energy Lett* 2023;8:4753-61. DOI
189. Liao J, Zhang F, Lu Y, et al. Sodium compensation and interface protection effects of Na_3PS_3O for sodium-ion batteries with P2-type oxide cathodes. *Chem Eng J* 2022;437:135275. DOI